Alexandria Engineering Journal (2022) 61, 7315–7337

HOSTED BY

Alexandria University

Alexandria Engineering Journal

www.elsevier.com/locate/aej
www.sciencedirect.com

A critical review on the thermal performance of alternating cross-section tubes

Amawasee Rukruang [a], Nares Chimres [b,c], Jatuporn Kaew-On [b,c], Mehrdad Mesgarpour [c], Omid Mahian [d,e], Somchai Wongwises [c,f,*]

[a] Energy Engineering Program, Faculty of Engineering, Thaksin University, Phatthalung 93210, Thailand
[b] Mechanical Engineering Program, Faculty of Engineering, Thaksin University, Phatthalung 93210, Thailand
[c] Fluid Mechanics, Thermal Engineering and Multiphase Flow Research Lab. (FUTURE), Department of Mechanical Engineering, Faculty of Engineering, King Mongkut's University of Technology Thonburi (KMUTT), Bangmod, Bangkok 10140, Thailand
[d] School of Chemical Engineering and Technology, Xi'an Jiaotong University, Xi'an, China
[e] Department of Mechanical Engineering, Center for Nanotechnology in Renewable Energies, Ferdowsi University of Mashhad, Mashhad, Iran
[f] National Science and Technology Development Agency (NSTDA), Pathum Thani 12120, Thailand

Received 8 September 2021; revised 12 December 2021; accepted 28 December 2021
Available online 20 January 2022

KEYWORDS

Alternating cross-section tube;
Deformed tube;
Enhanced tube;
Heat transfer enhancement;
Multi-longitudinal vortices;
Vortex generation

Abstract This paper aims to summarize publications related to new generation of tube geommetry, thermal performance, and flow characteristics in different cross-sectional manners, and the effect of crucial parameters on thermal–hydraulic performance. An alternating cross-sectional tube has an enhanced vorticity without installing vortex generator devices. Multi-longitudinal vortices are induced along the length of the tube: this makes a significant enhancement in the thermal performance of the tube. Many published papers have focused on the heat transfer and flow characteristics of the alternating cross-section tubes in various configurations in the past two decades. Although the cross-sections had different shapes, the flow behaviors and vortex generation were similar. The geometric parameters, like aspect ratio, pitch length, transition length, alternating angle, phase-shifting, and the total length, influenced the thermal–hydraulic performance of the alternating cross-section tube. The flow characteristics in an annular region differed between the alternating cross-section tube as internal and external tubes. Moreover, some researchers proposed the Nu and f correlations for the practical design of heat exchangers. Finally, future research works and improvement guidelines for alternating cross-section tubes are revealed.

* Corresponding author at: Fluid Mechanics, Thermal Engineering and Multiphase Flow Research Lab. (FUTURE), Department of Mechanical Engineering, Faculty of Engineering, King Mongkut's University of Technology Thonburi (KMUTT), Bangmod, Bangkok 10140, Thailand.
E-mail address: somchai.won@kmutt.ac.th (S. Wongwises).

Peer review under responsibility of Faculty of Engineering, Alexandria University.

https://doi.org/10.1016/j.aej.2021.12.070

Nomenclature

ACFT	Alternating cross-section flattened tube
ACT	Alternating cross-section tube
AEAT	Alternating elliptical axis tube
AFT	Alternating flattened tube
AR	Aspect ratio
DET	Deformed external tube and smooth core
DETSC	Deformed external tube and swirling core
ER	Enhancement ratio
HTC	Heat transfer coefficient
HTR	Heat transfer rate
MLV	Multi-longitudinal vortices
PEC	Performance evaluation criteria
SC	Smooth external tube and swirl core
TL	Transition length
TS	Transition section

Symbols (and units)

D	Tube diameter (mm)
D_h	Hydraulic diameter (mm)
f	Friction factor (-)
h	Inner tube height (mm)
L	Tube length (mm)
Nu	Nusselt number (-)
P	Pitch length (mm)
Pr	Prandtl number (-)
Re	Reynolds number (-)
r	Reynolds number ratio (-)
V	Velocity (m/s)
w	Inner tube width (mm)
θ	Alternating angle (°)
ΔP	Pressure drop (Pa)
β	Angle between fluid velocity vector and temperature gradient (°)
ϕ	Less longitudinal Phase-shifting (-)
λ	Deformation wavelength (-)
∇T	Temperature gradient (-)
V	Velocity vector (-)
$V \cdot \nabla T$	Coordination of the velocity and temperature fields (-)

Subscripts

a	Major axis
anl	Annular area
avg	Average
b	Minor axis
bf	Base fluid
f	Working fluid
e	Enhance tube
i	Internal
loc	Local
max	Maximum
min	Minimum
nf	Nanofluid
o	External
oa	Overall
s	Smooth tube
t	Transition
w	Water

Contents

1. Introduction

For academic researchers and thermal technicians in the industry, the perennial subject of enhancing heat transfer has always been an attractive study. Three enhancement techniques can improve the performance of the heat exchanger [1]). First, it

is possible to introduce active techniques to increase the heat transfer rate (HTR) of the heat exchanger. The techniques include jet impingement, fluid vibration, mechanical aids, electrostatic fields, and surface vibration [2–4]. The active method shows that an increase in HTR involves a relatively constant space occupied by the tube and pressure drop (ΔP). However, adding an external power supply is a major cost of enhancing heat transfer in this way.

Second, passive technology does not require the system to use an external power source. Enhancement by passive technology can change the structure of the tube or the properties of the working fluid, for example, rough surfaces, extended surfaces, swirl flow devices, coiled tubes, liquid additives, gas additives. As mentioned above, passive techniques are divided into two different categories: (i) improving the thermodynamic properties of the working fluid and (ii) modifying the heat exchanger tube structure. The working fluid properties can be improved by adding nanoparticles to the base fluid [5–6]. This method enhances not only the fluid thermal conductivity but also increases convective heat transfer. However, the cost of nanoparticles is the main obstacle to realizing this method [7]. The other method consists of changing the tube structure, which can be achieved by changing the geometry of the tube or inserting extra parts into the heat exchanger tube [8–9]. These methods induce secondary flow and increase the intensity of turbulence in the tube. However, these two factors lead to an increase in HTR and ΔP. Further, due to modification in its structure, the space occupied by the tube may change [10].

The last enhancement technique is compound technology, in which two or more active and/or passive techniques can be implemented together, such as active-active, active–passive, or passive-passive techniques. These methods are more effective than using a single technique. A number of studies have involved compound passive-passive enhancement because the passive method shows satisfactory heat transfer improvement without requiring increased external power. Examples include a combined wedge-ribbed tube with a winglet vortex generator, a coiled corrugated tube, an axial corrugated tube with a helical screw-tape insert, a corrugated tube with twisted tape insert, and a rectangular channel with a combined delta winglet insert, etc. [11–15].

This paper focuses on passive enhancement techniques related to changing tube geometry categories. A tube structure with an alternating cross-section of its tube is introduced. The alternating cross-section tube (ACT) is made from a circular tube. The evolution of the tube is developed from a flattened tube and then reshaped to an ACT by turning its cross-section. Each alternating cross-section is connected by a transition section (TS). Consequently, the ACT generated a secondary flow without installing vortex generator devices. Evidently, multi-longitudinal vortices (MLV) plays an important role in enhancing heat transfer. The authors intend to collect literature related to the ACT from 2003 to the present. The number of related papers about 20 years can be revealed into two periods: the first one is from 2003 to 2008, and the second is the year 2014 to the present, as demonstrated in Fig. 1. It should be noted that the related research conducted during the past five years could not be found in open literature. Two main categories found in the open literature: flow in a single tube and flow in a concentric tube, are examined by numerical studies. An experimental approach is found in only one work. Most researchers paid attention to a single tube investigation. While a few researchers emphasized on a concentric tube study. In this paper, the authors intensively focused on the thermal–hydraulic performance of the ACT in all aspects. Therefore, this paper aims to provide a comprehensive review of conceptual tube design, heat transfer and flow resistance characteristics, tube performance, tube geometric parameters, future research works, and improvement guidelines for ACT. Also, the latest technology in the ACT is reported and comprehensively analyzed. All investigation details are explained and discussed in Sections 3 and 4.

2. Overview of the ACT investigations

Conventional circular tube, which is associated with a tube hydraulic diameter of greater than 6 mm, has commonly been used in heat exchangers in various applications. However, they are not satisfactory because the area of contact surface per unit volume is small, resulting in a heat exchanger size that is too large. It affects the material cost, installation area, and amount of working fluid in the system. Consequently, several researchers have paid attention to improving thermal performance of the conventional circular tube. A simple way to improve the performance is to modify the tube geometry. Flattening the circular tube helps increase the heat transfer by affecting the flow pattern. Many published articles suggest that the thermal performance of flattened tubes is better than those of circular tubes [16–18].

In 1998, Guo et al. [19] discovered three novel approaches for convective heat transfer augmentation of parabolic flow. One relies on the principle of field synergy, which consists of an increase in the angle between the non-dimensional velocity and temperature gradient vectors. To improve the performance of the flattened tube, an alternating cross-section of the tube is the next step in the tube modification. The ACT was designed based on the field synergy principle. The main characteristics of ACT (Fig. 2) are: (i) the core fluid in the tube is closer to the tube surface, which leads to an increase in the HTR between the fluid and the tube surface; and (ii) an increase in turbulence intensity leads the boundary layer to increase fluid mixing. Three parameters affect the heat transfer performance of the ACT. The first is the distance between the two transition sections (pitch length, P), which causes the flow characteristics to change. The second is the ratio of the width to the height of the flattened section (aspect ratio, AR), which is related to the flow passage of the tube. When the tube becomes thinner, the core fluid comes closer to the tube wall. Finally, the transition section length (TL) is to impose the flow characteristic before it reaches a constant area. The conceptual design of ACT is displayed in Fig. 3.

Fig. 4 shows the coordination relationship between flow velocity and temperature distribution. For the elliptical cross-section, the synergy between the velocity vector and temperature gradient is not very good because the local velocity is more or less parallel to the local temperature gradient. In contrast, combining alternating elliptical cross-sections, MLV structure, and deformed temperature field leads to an increase in the heat transfer coefficient (HTC) because most of the local temperature gradient is parallel to the local velocity [20].

The alternating section of the tube is produced from a circular tube. The tube is composed of cross-sectional segments connected to its cross-section or another cross-section by means of a rotation angle between those segments. The connection between the two segments is called the TS. The tube

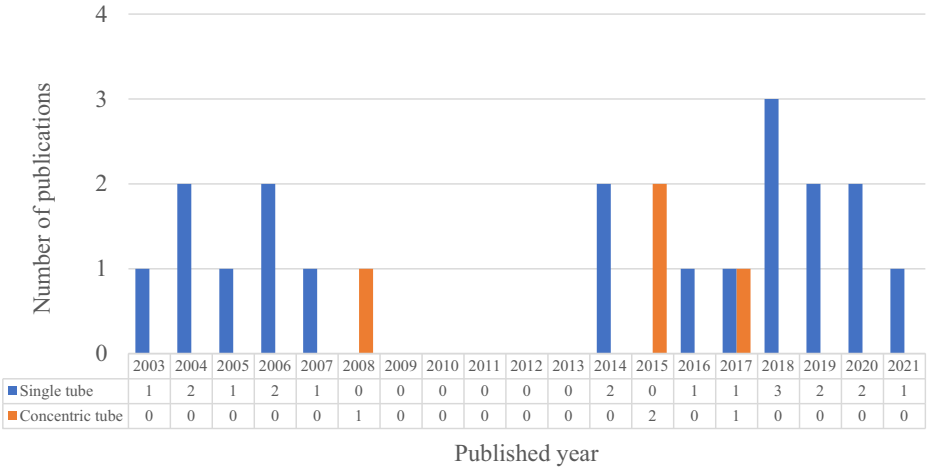

	2003	2004	2005	2006	2007	2008	2009	2010	2011	2012	2013	2014	2015	2016	2017	2018	2019	2020	2021
Single tube	1	2	1	2	1	0	0	0	0	0	0	2	0	1	1	3	2	2	1
Concentric tube	0	0	0	0	0	1	0	0	0	0	0	0	2	0	1	0	0	0	0

Fig. 1 Number of publications of the ACT from the year 2003 to 2021.

arrangement is defined by each alternate cross-sectional segment, which is connected at an angle of rotation (usually 90°) along the length of the tube. The AEAT cross-section is an ellipse or oval characteristic that connects its cross-section through various rotation angles, as shown in Fig. 2. ACTs are developed on the basis of the field synergy principle. It is possible to generate MLV without installing the generator on the tube surface. Therefore, the vortex is induced by an alternating cross-section of the tube which results in the generation of secondary flow and turbulence intensity. Guo [21] designed an AEAT based on the principle of field synergy compared with a circular test tube. He found that the HTR increased by approximately 300%, and the ΔP moderately increased, about 30%-120%. The results revealed satisfactory heat transfer performance and economic potential for the tube configurations.

Besides, Pauley and Eaton [22] reported that MLV induced fluid flow to the wall, then caused fluid to return to the middle tube, destroying the thermal boundary layer and resulting in a crucial improvement in the HTR.

Table 1 summarizes all essential research on ACTs. There are both single tube and concentric tube studies on the thermal-hydraulic performance of tubes with alternating cross-sections. Most of the studies focus on the numerical investigation. There is only one that was performed by an experimental method. Obviously, a single tube test was widespread in the study area. However, a few studies have focused on concentric tubes.

3. Single tube

The numerical approach was a popular method to assess the heat transfer and pressure drop characteristics of the ACTs. Conversely, the experimental method appeared in the open literature, primarily applied to the validation procedure. Only one experimental work was presented by Sajadi and Talebi [23]. The work was related to investigating the nanofluid flowing through the alternating cross-section flattened tube (ACFT). All investigations were performed on a single-phase condition, which used water, oil, air, glycol/water, Al_2O_3/water, and ZnO/water as a working fluid. In this section, the noticeable parameters on the thermal–hydraulic performance of the ACT were analyzed and assessed, such as (i) tube geometry, (ii) P, AR and TL, (iii) alternating angle, and (iv) miscellaneous parameters. Also, the proposed correlations were gathered and presented.

3.1. Effect of tube geometry on the thermal–hydraulic performance

Two different cross-sections were indicated as an elliptical or oval cross-section and a flattened cross-section. A number of researchers carried out work on the AEAT, in which an elliptical or oval cross-section. It can be explained that the eddy flow was generated from the edge of the major axis, as illustrated in Fig. 5 (for the AEAT) and Fig. 6 (for the ACFT). In the fully developed flow region, the vortices were completely formed at the edge of the wall [24]. In addition, an increase in Reynolds number (Re) directly affects the flow characteristics, leading to an enhancement in the intensity of vortices. The flow behaviors directly impact the heat transfer enhancement. That is because of a well-mixed fluid at the tube wall. Fig. 5 shows the flow velocity in the AEAT at different Re. The figure presents that the four-soft vortices occurred at the Re = 200, and the eight-strong vortices occurred at the Re = 20000. However, it seems that the transition flow regime was at Re = 2000 [20]. That is similar to the generation of eddy flow in the ACFT, as displayed in Fig. 6. At Re = 500, the four vortices were formed at the edge of cross-section. Evidently, at this Re, the velocity and thermal boundary layers were large. As a result of the uniform velocity in the middle of the tube and near the walls, the heat transfer coefficient decreased. By increasing Re from 500 to 750, another eddy flow was generated in the opposite direction to the previous one. It can be seen that the temperature variation of cold fluid in the middle of the tube corresponded with the primary vortices. At Re = 1,000, the secondary vortices were clearly visible. It was confirmed that at this Re, the generated vortices had an effect on the temperature distribution.

Eight vortices were formed when the Re > 1000. The eddy flow became more extensive at Re = 1,250. The vortices induced the core fluid to move toward the tube wall. The velocity and temperature distributions were revealed in a diagonal shape. The fluid mixing in the cross-section leads to an increase

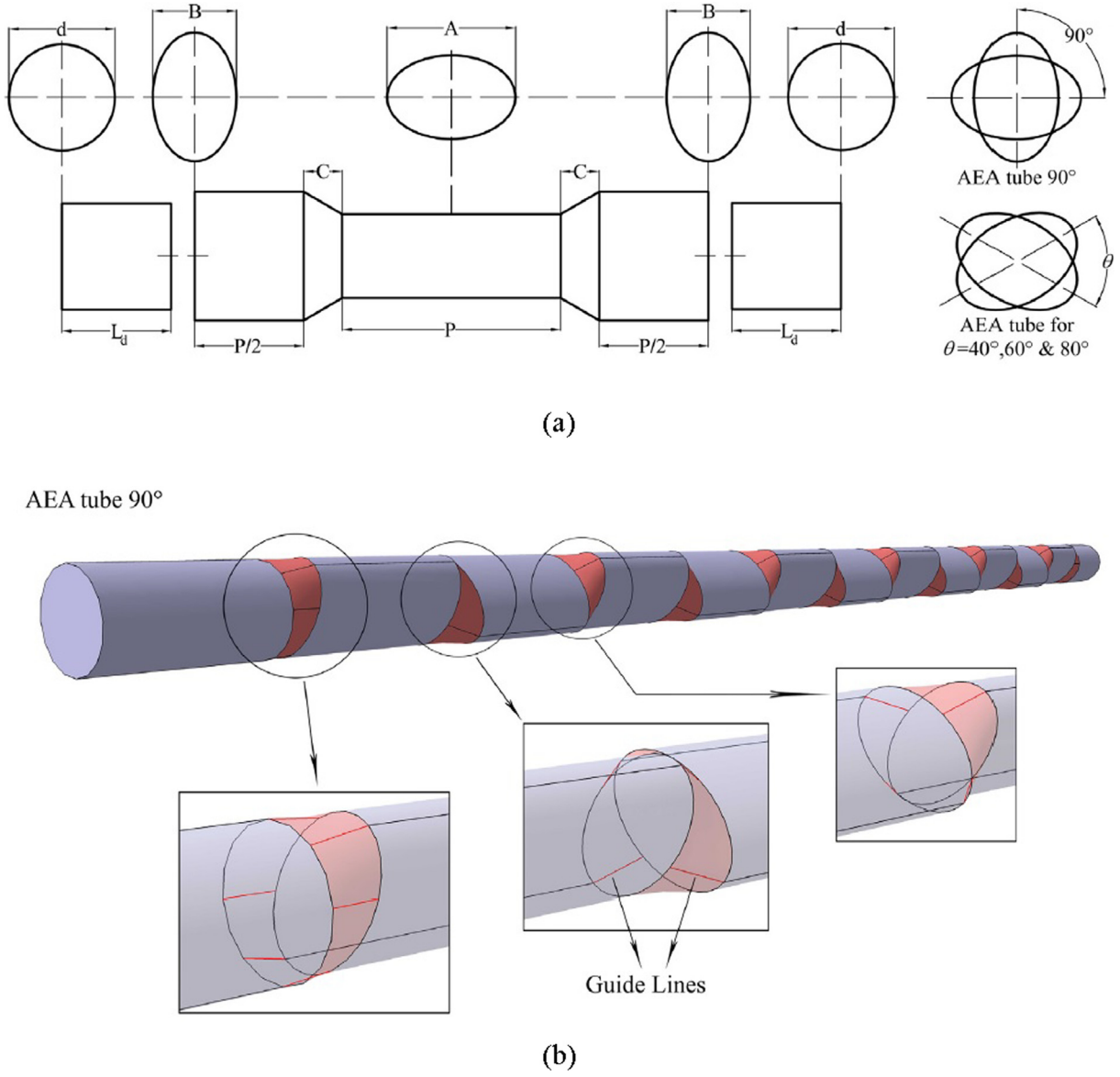

Fig. 2 The geometry of alternating elliptical axis tube (AEAT) with various rotation angles: (a) 2D geometry, and (b) 3D geometry of the AEAT with an alternating angle of 90° [From Khaboshan and Nazif [35], with permission from Elsevier].

in heat transfer performance. At Re = 1,500, the vortices were more intensive and this was the primary reason for the increased heat transfer at high Re [25].

As a result, the ACT can generate vortex without installing vortex generator devices. The vortices were induced by contraction, and expansion of tube geometry along the tube which led to changing flow behavior. Meng et al. [26] informed that variation of the tube surface influenced the flow velocity vectors and the temperature distributions in the AEAT. Due to the eddy flows, the MLV created a well-mixed fluid near the surface of the tube. The fluid was then moved through the middle of the cross-section. This phenomenon was the origin of the notable change in the temperature field. The combination of flow and temperature fields improved heat transfer, preferably in a low Re range. Sajadi et al. [10] proposed a novel type of tube with ACT. The tube was developed from an ACFT, and by replacing some elliptical segments with a circular part. The tube pattern consists of a flattened cross-section alternating with a circular cross-section along the tube length, and the tube is called an alternating flattened tube (AFT). They used the numerical model to determine the heat transfer mechanism of the AFT. The results revealed that the vortex intensity increased in the TS. An increase in vorticity magnitude improved not only the local heat transfer coefficient (HTC_{loc}) at the TS but also enhanced the overall heat transfer coefficient (HTC_{oa}) of the AFT. For this reason, the HTC and ΔP of the AFT were higher than those of a round tube. Moreover, under the same ΔP, AFT can improve thermal performance by 41% compared to circular cross section tubes.

Khaboshan and Nazif [27] performed a numerical analysis of air convective turbulence in AEATs. The simulation results show that the axial vortex was induced in the AEAT, which led

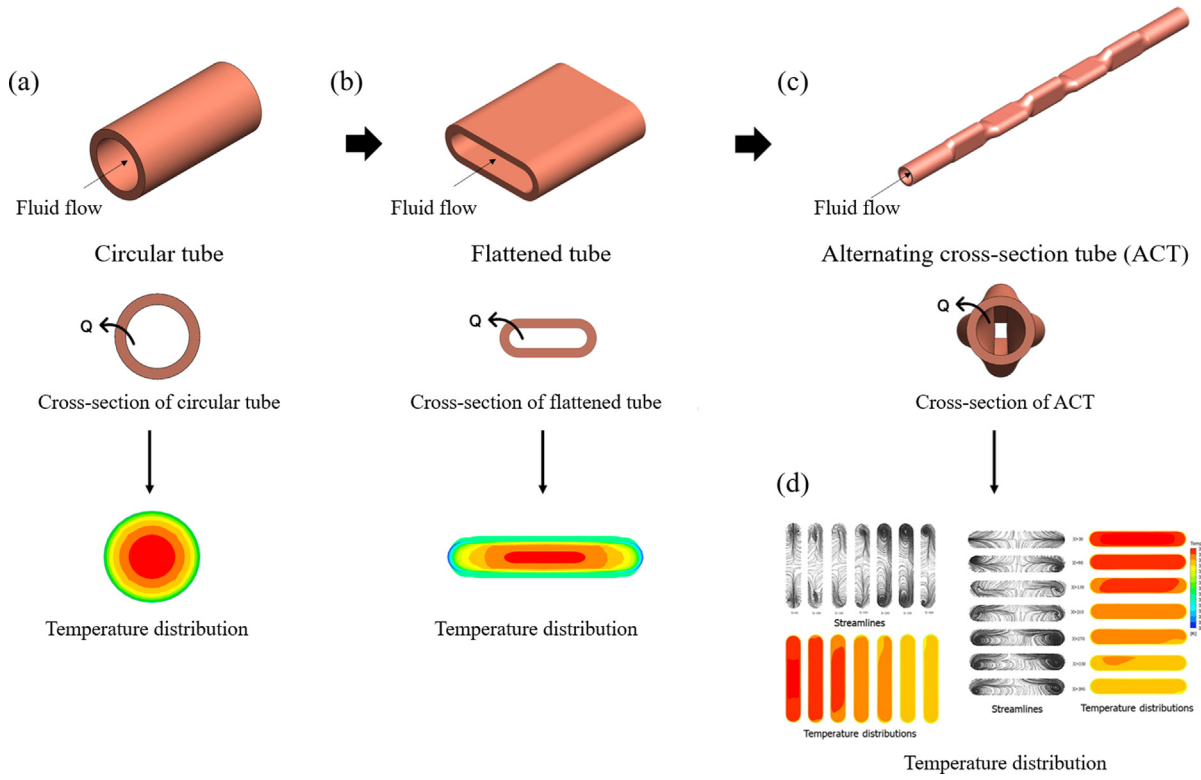

Fig. 3 Conceptual design of ACT: (a) circular tube, (b) flattened tube, (c) ACT, and (d) velocity vectors and temperature distribution of ACT by Rukruang et al. [24], with permission from John Wiley and Sons.

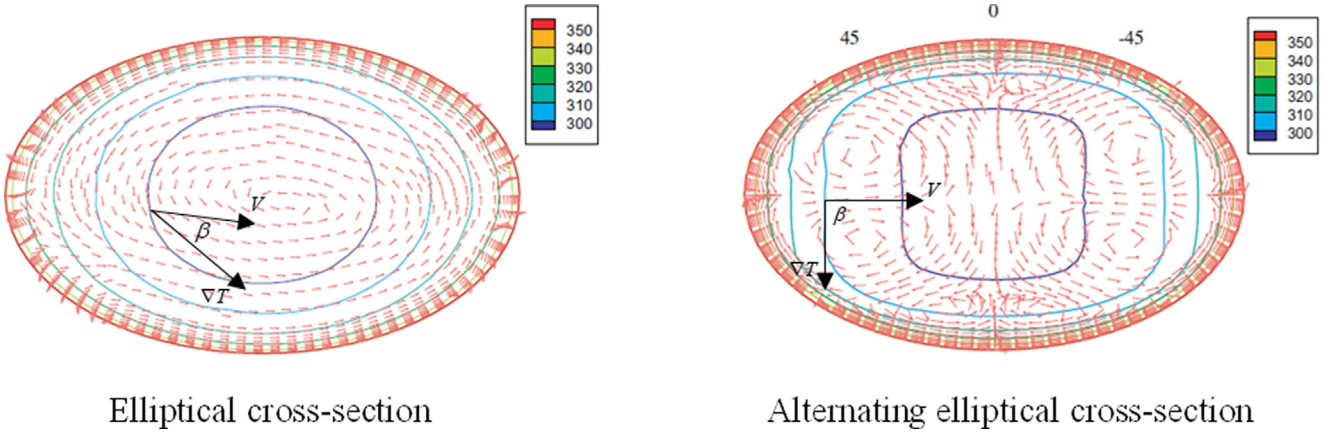

Fig. 4 Streamlines and temperature distributions in an elliptical cross-section and alternating elliptical cross-section [From Li et al. [20], with permission from Elsevier].

to an increase in HTC and ΔP. From this perspective, the MLV greatly influenced the temperature gradient, which explains the significant increase in HTC. Besides, Khaboshan and Nazif [28] examined the Al_2O_3-water nanofluid flowing inside an AEAT using a two-phase mixing model under constant wall temperature conditions. The flow structure inside the AEAT was analyzed by numerical simulation. Reverse flow appeared in the TS, resulting in a bubble separation in the region near the wall. The reverse flow existed continuously after the transition region. The MLV appeared on the main diagonal of the AEAT, and the cross-sectional area of this section was reduced. Although the HTC was improved, the generation of eddy currents also increased the ΔP. As a result, a geometric shape can be designed to minimize flow resistance in the transition zone, thereby avoiding separation.

Moreover, Li et al. [20] depicted that the temperature gradient of the AEAT deformed at the edge of the long axis: when the Re increased, the deformation became more obvious.

Table 1 The summary of the essential research on the ACTs.

Authors	Type of study	Tube geometry	Application	Reynolds number	Working fluid	Tube diameter	Remarkable findings
Chen et al. (2004)	Numerical work	AEAT	Single tube	10,000–60,000	Water	D_i = 16.5 mm	The TS is the key to improve HTC; also, the ΔP increases at the same time.
Meng et al. (2005)	Experimental and numerical works	AEAT	Single tube	500–50,000	Deionized water and lubricant oil	D_i = 17.0 mm	The MLV generation is the main effect of augmenting heat transfer performance, which is generated by tube geometry as the contraction and expansion along the tube length.
Chen et al. (2006)	Numerical work	AEAT	Single tube	$\leq$ 2,000	Water	D_i = 16.5 mm	A problematic design for a wide range of Re; on the other hand, it could be possibly optimized designed at a fixed Re.
Li et al. (2006)	Numerical work	AEAT	Single tube	200–2,000	Air	D_i = 17.0 mm	The transition from laminar flow regime to turbulent flow regime occurs at an early Re of 1,000.
Chen (2007)	Numerical work	AEAT	Single tube	100–2,000	Water	D_i = 16.5 mm	The wall temperature distribution varies along the tube circumferential direction and the tube axial direction.
Khaboshan and Nazif (2017)	Numerical work	AEAT	Single tube	5,000–20,000	Air	N.A.	MLV has a significant impact on the temperature gradient, resulting in a dominant enhancement of heat transfer.
Khaboshan and Nazif (2018)	Numerical work	AEAT	Single tube	10,000–60,000	Al_2O_3-Water	D_i = 16.5 mm	The total entropy generation increases with increasing nanoparticle volume fraction and decreasing nanoparticle diameter.
Khaboshan and Nazif (2018)	Numerical work	AEAT	Single tube	10,000–60,000	Water	D_i = 16.5 mm	The number of MLV increases from 4 to 8 by increasing the angle of θ from 60° to 80°.
Khaboshan and Nazif (2018)	Numerical work	AEAT	Single tube	10,000–60,000	Water	D_i = 16.5 mm	With an increase in the θ, the velocity gradient is transferred owing to the secondary flow generation.
Khaboshan and Nazif (2019)	Numerical work	AEAT	Single tube	10,000–60,000	Water	D_i = 16.5 mm	A synergy between velocity and temperature field can be enhanced convection heat transfer. One way to improve field coordination is the creation of MLV in the fluid.
Sajadi et al. (2014)	Experimental and numerical works	ACFT	Single tube	300–2,000	Oil	D_i = 14.62 mm	Either increasing the AR or decreasing the P tends to increase the HTC and ΔP.
Zambaux et al. (2014)	Numerical work	AEAT	Single tube	828	30% mixture of glycol and water	D_m = 10.0 mm	The A and the λ have an essential effect on heat transfer phenomena within the tube.
Rukruang et al. (2019)	Experimental and numerical works	ACFT	Single tube	1,000–4,000	Water	D_i = 4.25 mm	The entrance length of the turbulent flow was longer than that of the laminar flow as the susceptible turbulent flow deviates from the change of the cross-section of the tube.
Khaboshan and Nazif (2020)	Numerical work	AEAT	Single tube	10,000–60,000	Water	D_i = 16.5 mm	The AEAT having θ of 90° is the best performance for Re 10,000. In contrast, the AEAT performance is lower than the circular tube in the Re greater than 20,000.
Sajadi and Talebi (2020)	Experimental work	ACFT	Single tube	400–1900	ZnO/water	D_i = 14.62 mm	An increment in the concentration of nanofluid leads to increasing HTC and ΔP.
Farsi et al. (2021)	Numerical work	ACFT	Single tube	500–1500	Water	D_o = 9.5 mm	The AR has the highest effects on the thermal–hydraulic performance, followed by the TL and P.
Sajadi et al. (2016)	Experimental and numerical works	AFT	Single tube	500–2,000	Oil	D_i = 14.62 mm	An increase in vorticity magnitude improves both the HTC_{loc} at the TS and enhances the HTC_{oa} of the AFT.

(*continued on next page*)

Table 1 (*continued*)

Authors	Type of study	Tube geometry	Application	Reynolds number	Working fluid	Tube diameter	Remarkable findings
Chen and Dung (2008)	Numerical work	AEAT	Concentric tubes	$\leq$ 2,000	Water	D_i = 16.5 mm	The Re_i was a higher effect on the HTC than the Re_o.
Zambaux et al. (2015)	Numerical work	AEAT	Concentric tubes	388	30% mixture of glycol and water	$D_{h,anl}$ = 5.0 mm	An external wall deformation induces the vortices generation; on the contrary, the tangential velocity vectors at the internal deformations appear in opposite directions.
Zambaux et al. (2015)	Numerical work	AEAT	Concentric tubes	448	Water	$D_{h,anl}$ = 5.0 mm	Combining the external wall deformation and internal swirling tubes have a proper mixing, leading to an augment in the heat and mass transfer.
Vaezi et al. (2017)	Numerical work	AEAT	Concentric tubes	100–1,600	Water	D_i = 16.5 mm	The HTR enhances with increasing AR. The phenomenon is more sensitive for Re higher than 600, while Re lower than 100 cannot be achieved.

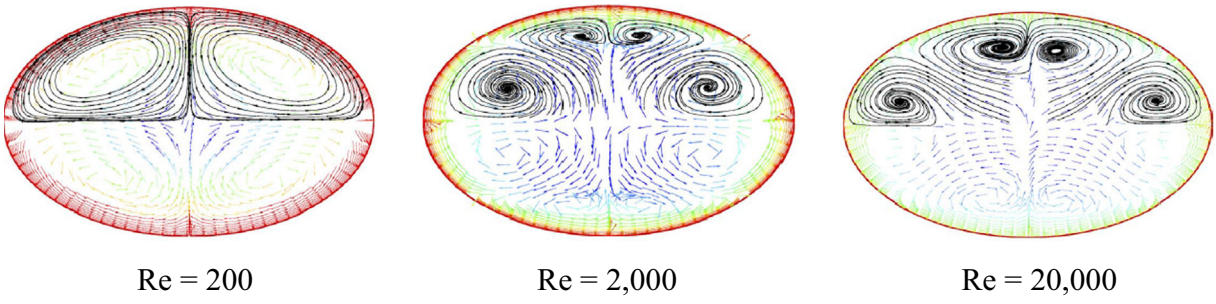

Fig. 5 Vortex structure of AEAT cross-section [From Li et al. [20], with permission from Elsevier].

Combining the MLV structure and the deformed temperature field led to an augmentation in heat transfer because most of the local temperature gradient was parallel to the local velocity. Also, the temperature distribution consisted of the velocity field, in which the temperature was growing from the wall to the core fluid in the middle tube. Farsi et al. [25] mentioned that the wall temperature dramatically decreased when the Re increased, as shown in the dot plot in Fig. 6.

Chen et al. [29] numerically studied the flow and heat transfer behavior of water flowing through an AEAT with a low Re. The tube dimensions were represented by L_t, D_b (minor axis), D, D_a (major axis), and L equal to 6, 13, 16.5, 20, and 40 mm, respectively. Eight positions along the axial direction were examined for flow characteristics and temperature distribution. These positions were defined as 0.01, 0.075, 0.125, 0.175, 0.2, 0.325, 0.45 and 0.575L, which were represented by Locations 1 to 8, respectively. The eight investigated positions along the axial direction are illustrated in Fig. 7. As mentioned, the first three positions were in the TS.

The velocity vectors and pressure contours for eight positions are provided in Fig. 8. At the Re = 20000, the simulation results indicated that the secondary flow in a horizontal elliptical position was smaller than that of the TS. The velocity vectors for Locations 5 through 8 were 1.6 times the value of the first four locations. The investigation section was a location that changes from a vertical oval cross-section to a horizontal oval cross-section. location 1 was a compressed shape, which initially placed high pressure on the initial position while placing low pressure at last, as shown in location 2. The different pressures induced violent secondary flow, which can drive fluid from regions 1 to 2. At Location 3, the cross-section was gradually compressed due to the last stage of the TS. The secondary flow occurred continuously over a short length downstream and at the end of the TS. Additionally, the secondary flow decreased rapidly along the horizontal oval cross section of locations 6-8, whereas the primary flow was constant. At the same time, the eddy current developed smoothly due to developing close to the vertical oval cross-section (Location 1). According to the analysis, the TS was the primary key to generating the driving force of the secondary flow. The bubble separation occurred as an immediate contraction and discontinuous curvature geometry at the end of the TS. Additionally, an extended geometry resulted in a large region of separation in the area adjacent to the wall at location 2 and through a constant area section. The appearance in the separation regions is depicted in Fig. 9. This separation was called near-wall bubble separation. Heat transfer can be affected by reverse flow. The bubble separation reduced the overall performance of the tube to a certain extent. Accordingly, the axial bubble separation had to be eliminated to increase the overall performance of the tube. The authors also reported that the heat transfer enhancement at a low Re was more significant than that at a high Re. The HTC increased from 40% to 100% depending on the Re, whereas the pressure loss penalty increased twice as much as that of a circular tube. Chen and Fang [30] pointed out, through computational investigation,

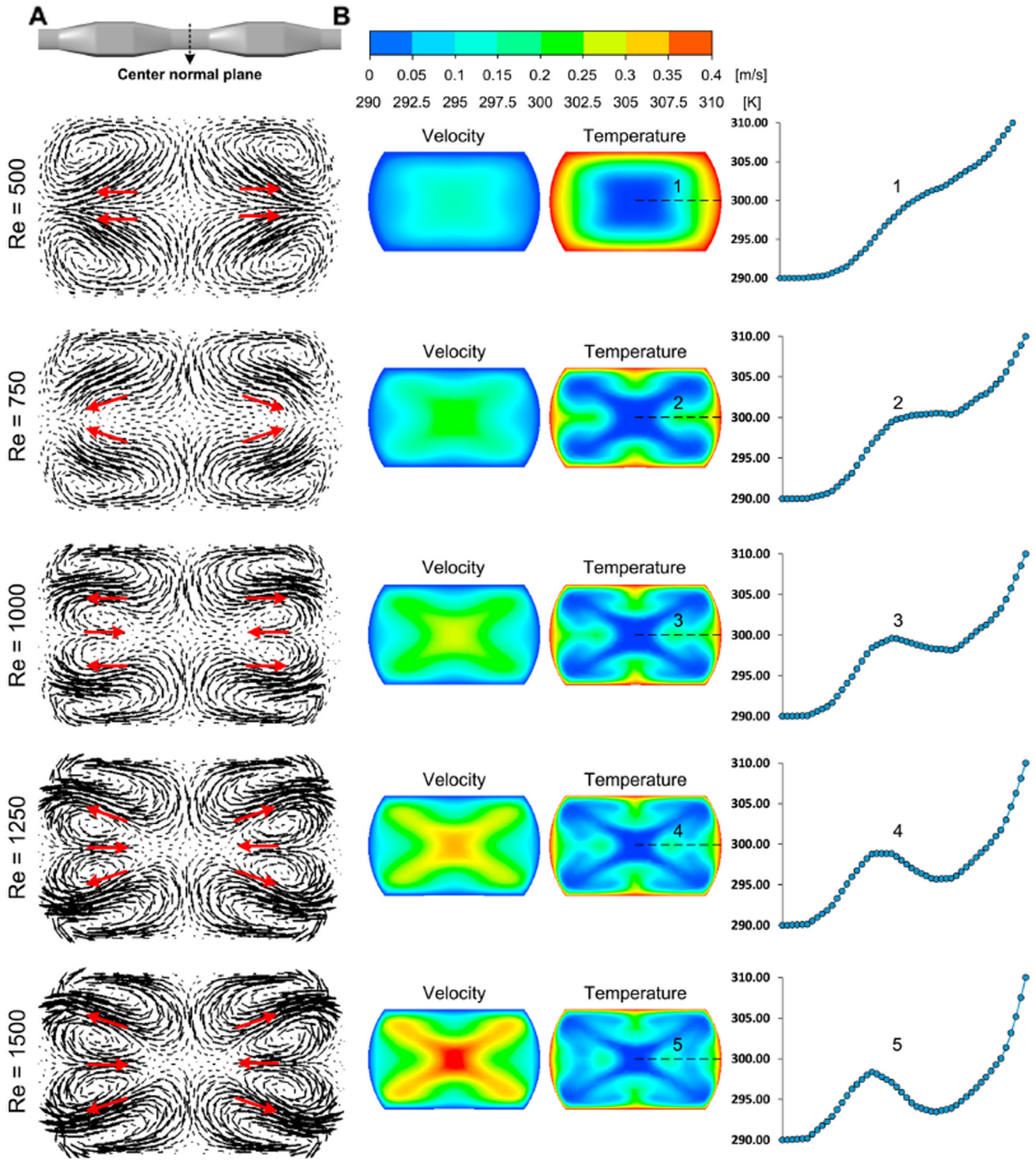

Fig. 6 Velocity generation and temperature distribution of ACFT cross-section [From Farsi et al. [25], with permission from Elsevier].

that the heat transfer enhancement of the AEAT was as high as 600% compared with the circular tube.

Also, Chen [31] analyzed the heat transfer characteristics of the AEAT, which was placed in a cross-stream. The computational domain was selected based on a single tube due to a phenomenon similar to the others. Two different Reynolds numbers were defined as an internal Reynolds number (Re_i) and an external Reynolds number (Re_o). The temperature contours on an exterior wall with the Re_i of 1,000 and Re_o of 40 were visible, as the temperature of the wall sharply changed the circumferential and axial directions, as presented in Fig. 10.

Due to the higher temperature difference between fluid and tube surface on this side, as well as the thinner boundary layer thickness on the tube, the thermal resistance was lower and cooling rates were higher. Behind the tube, the region had

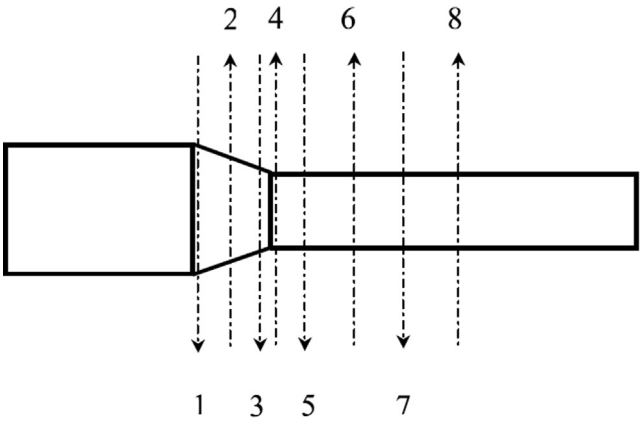

Fig. 7 The eight investigated positions along the axial direction [From Chen et al. [29], with permission from Elsevier].

lower cooling. Firstly, the cold fluid was already heated, so its capacity to remove heat from the tube wall was lower when it reached this area. Recirculated flow occurred behind the tube region. The fluid recirculated in the wake region resisted the other fluid entering into the wake region. This prevented fresh fluid from flowing into this area. Consequently, the fresh fluid in this area was unable to absorb the heat from the tube. This resulted in low convection heat transfer.

Fig. 11 exhibits temperature contours and velocity vectors on horizontal and vertical cross-sections. Compared to the velocity vectors and temperature contours at the cross-section unit, the vertical cross-section took longer than the horizontal cross-section to crush the stream. Evidently, on the right side of the cross-section (downstream), there was a higher temperature than on the other side (upstream); This proved that the frontal area had cooling superior to that in the rear area. Besides the vertical section, the velocity vectors of the external flow generated a secondary flow behind the tube, resulting in better heat transfer.

3.2. Effect of P, AR, and TL on the thermal–hydraulic performance

The crucial geometric parameters of ACT, which affect the heat transfer and pressure drop characteristics, are P, AR, and TL. Whenever those parameters change, the flow behavior inside the tube also differs. Meng et al. [26] carried out a test on convection heat transfer in the AEATs. The AEATs with a P of 40, 50, and 60 mm were studied. Meng et al. found that the Nu increased as P decreased for both deionized water and lubricating oil. A decrease in P resulted in more alternating sections for the same tube length, which increased turbulent intensity. That is because the vortices were being created and intensified as the number of cross-sections changed. In addition, the vortex generation induced better mixing fluid inside the tube causing the increase in the HTR. Nu is a parameter that represents the heat transfer characteristic. Therefore, Nu increased with a decrease in P. For the friction factor (f), the results revealed that the f increased as the P decreased. A decrease in P led to flow obstruction. The turbulence intensity increased due to an increase in number of alternating cross-sections. Both flow obstruction and turbulence intensity affected the increasing of the f. The HTC improved from 100 to 500% as ΔP increased from 100 to 350% approximately.

Chen et al. [32] performed a computational simulation of the laminar flow in the AEAT. This study focused on the optimized design of the AEAT. Three parameters were studied, such as the AR, TL, and P. The authors were interested in a laminar flow regime ($500 < Re < 2000$). The results showed that an increase in the AR led to an increase in both the Nu and f. The AEAT performed better, where the AR value was 1.44 to

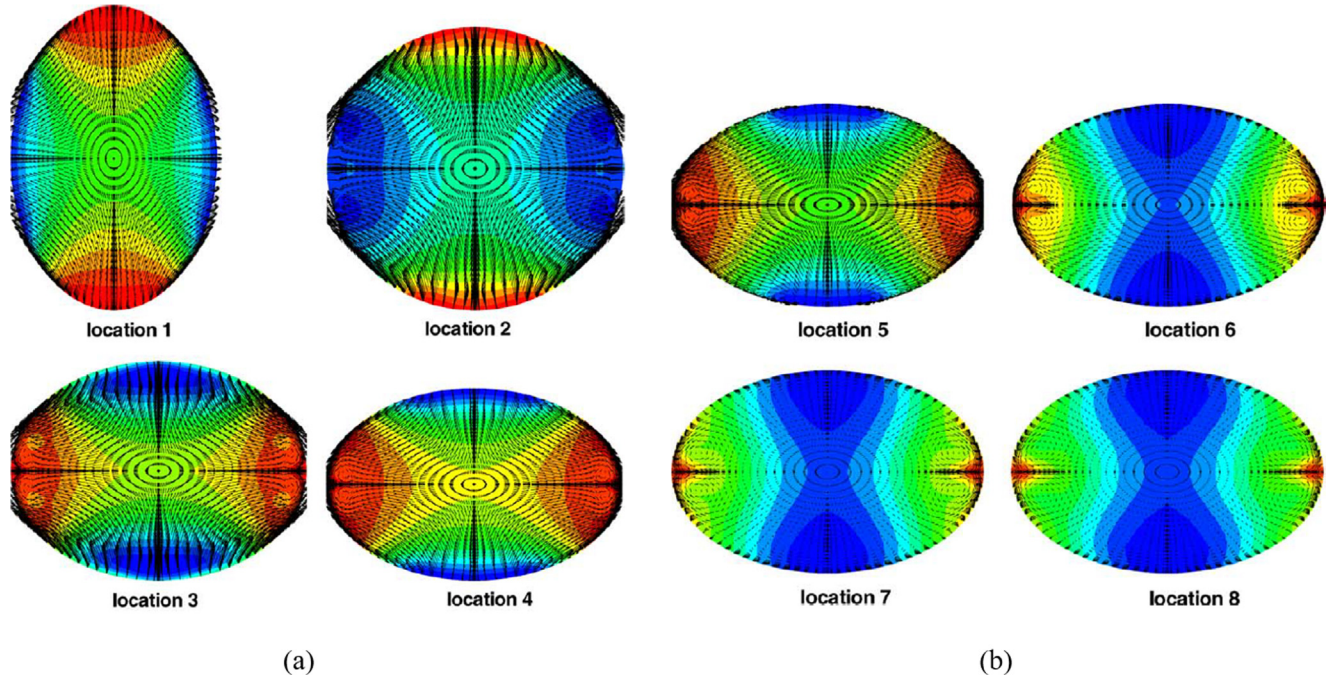

Fig. 8 Velocity vectors and pressure contours for eight locations: (a) locations 1–4, and (b) locations 5–8 [From Chen et al. [29], with permission from Elsevier].

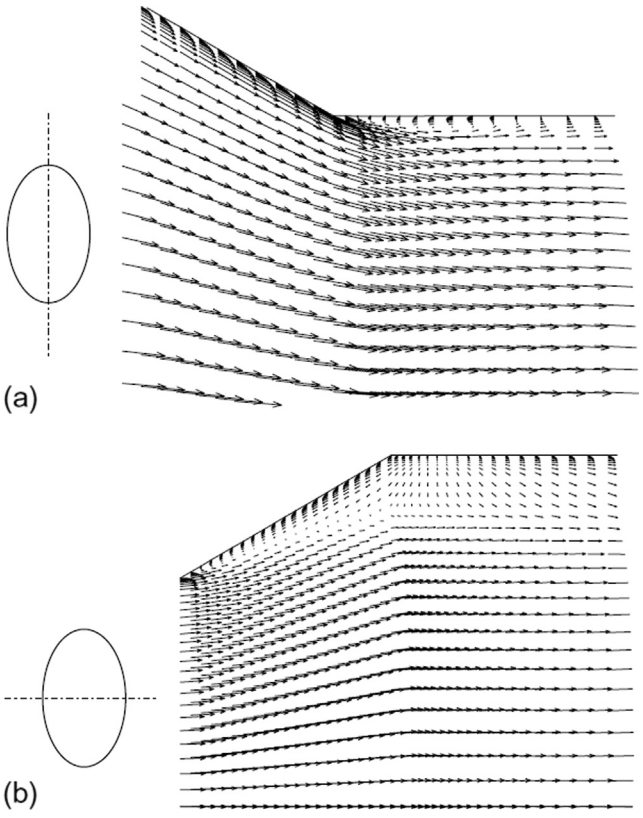

Fig. 9 Velocity vectors at axial tube: (a) contraction region, and (b) extension region [From Chen et al. [29], with permission from Elsevier].

1.64 in the Re ranges tested. Nu and f were reduced by stretching the TL. Similarly, the expansion of the P resulted in a decrease in the Nu and f.

Sajadi et al. [33] investigated the thermal-hydraulic performances of the oil flowing inside the ACFT. The ACFT was made of a copper circular tube with D_i of 14.615 mm. The study focused on the AR and P of the tube. The AR is an aspect ratio which is defined as its internal width (w) divided by its internal height (h): $AR = \frac{w}{h}$. It indicates the flatness of the tube. They obtained that an increase in the AR or a decrease in P led to an increase in HTR and ΔP. A decrease in P led to an increase in number of alternating sections which resulted in the increase of the flow obstruction, and turbulence intensity in the tube. Both flow obstruction and turbulence intensity led to increasing in ΔP. It can be clearly seen that ΔP increased with decreasing P. Sajadi and Talebi [23] conducted an experimental investigation of ZnO/water flowing in the ACFT. Three ACFTs with various AR, like 1.10 (Tube B), 1.12 (Tube C), and 1.14 (Tube D), were analyzed. A higher value of AR means the ACFT was more flattened. Oil was used as a base working fluid. In the test condition, the concentration of the nanofluid varied between 1 and 2%. The experiment revealed that adding the flatness of the tube resulted in an increment of HTR and ΔP relative to a circular tube. At Re of 400, the HTC of B, C, and D tubes were about 1.10, 1.43, and 1.55 times greater than the circular tube, respectively. Similarly, those values were 1.75, 2.7, and 3 times, respectively, for Re = 1800.

Farsi et al. [25] examined heat transfer and flow characteristics of ACFTs by various P, TL, and AR. The investigation was conducted using numerical analysis. Fluent V6 was

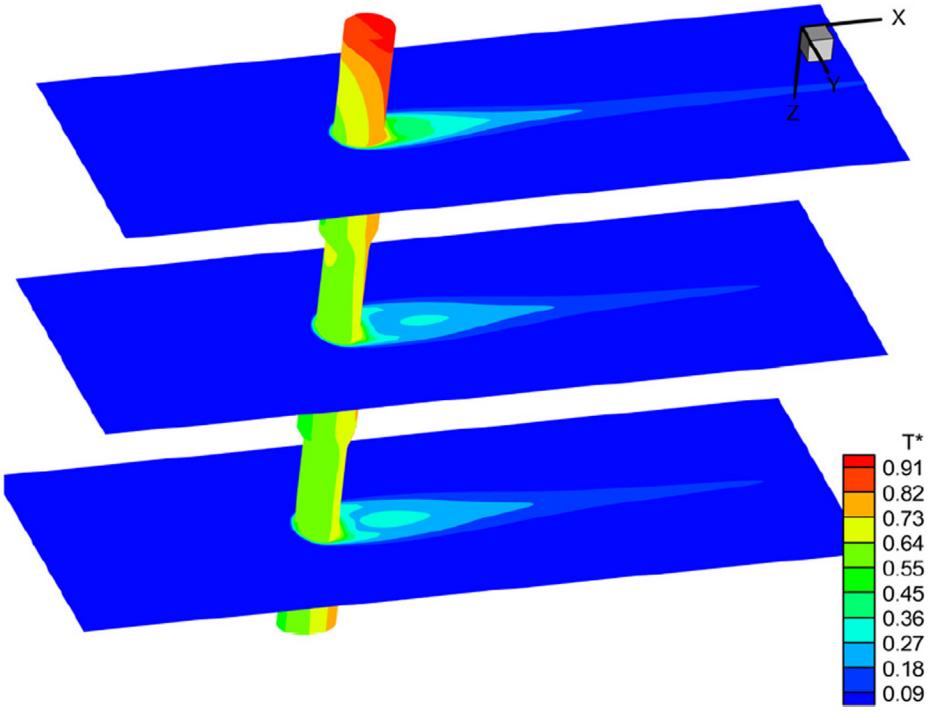

Fig. 10 Temperature contours on external wall of AEAT [From Chen [31], with permission from Elsevier]

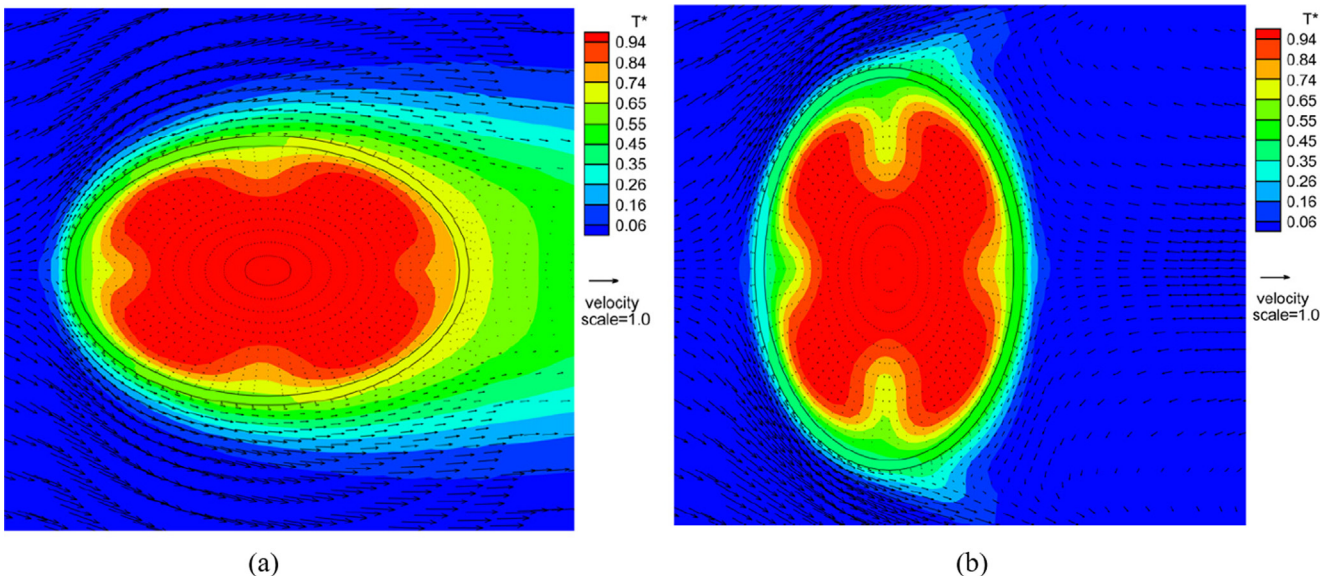

Fig. 11 Temperature contours and velocity vectors on: (a) horizontal elliptical cross-section, and (b) vertical elliptical cross-section [From Chen [31], with permission from Elsevier].

selected as the commercial software. Water was used as a working fluid in the Re range of 500 to 1500. The ACFT was made from a copper circular tube with D_o of 9.5 mm and L of 300 mm. In the parametric study, the AR had the greatest effects, followed by the TL and P. Compared to the circular tube, the Nu and f increased by changing P 1.34–3.21 and 2.78–4.91 times, by varying TL 1.23–4.45 and 2.75–7.50 times, and by altering AR 1.04–5.06 and 1.39–16.74 times, respectively. The ACFT with P of 10 mm, TL of 5 mm, and AR of 5 mm obtained the best performance in this study.

A vortex's size, shape, and location are affected by the transient length as illustrated in Fig. 12. The cross-section for primary and induced vortices grows as the transient length decreases. Additionally, the induced vortices shift towards the corners, and the shape of primary vortices changes from elliptical to diagonal. This results in more heat transfer near the walls. Fig. 13 shows the velocity distribution in a developed laminar flow does not differ too much from that in a straight tube. However, the thermal boundary layer grows quite quickly. In addition to the primary vortices, four induced vortices form as the minimum axis is reduced from 7.5 mm to 6.5 mm.

3.3. Effect of alternating angle on the thermal–hydraulic performance

Khaboshan and Nazif [34–36] conducted mathematical studies on the AEATs at different alternating angles (θ), as shown in Fig. 2. The investigation was carried out using water for $10000 < Re < 60000$. The middle cross-section of the TS varied from an elliptical to a square shape, from the θ of 40° to 80°. The middle region decreased as θ increased from 40° to 80°.

The velocity vectors and temperature gradients of AEATs with varying θ are shown in Fig. 14, which explains the phenomena in section c. In Fig. 14, the results reveal that the θ of 40° and 60° showed four vortices generation, whereas eight vortices generation occurred on the θ of 80° and 90°. Turbulent flow in the tube and the difference angle between input and output generated vortices at both ends of the tube. In addition, where tubes have greater angles θ, vortices occur due to an increase in pressure gradient. The cold fluid in the middle of the tube moved toward the tube wall in the direction of the streamlines. It resulted in the transfer of heat from hot fluid to the cold fluid in the middle of the tube. The presence of MLV encouraged fluid mixing, created a homogenized temperature gradient, and formed a thin boundary layer near the wall. As a result, heat transfer performance was enhanced.

Turbulent intensity represents the strength of the fluid mixture. At the exit of the TS, the turbulent intensity was higher than that of the others, in which the main axis exhibited vigorous turbulent intensity. Also, an increase in the θ led to an increase in the turbulent intensity. As illustrated in Fig. 14, the turbulent intensity is represented by the density of the vortices and the number of MLV that increased as the θ increased. The tube with θ = 40° and 60° generated four vortices, while the tube with θ = 80° and 90° generated eight vortices. By increasing the θ, the massiveness of the vortices obviously occurrs. The flow paths, which display the movement of hot and cold fluids through the tube are depicted in the figure. An increase in the θ resulted in the increase in the number of MLV and the massiveness of the vortices, leading to an increase in the turbulent intensity. However, this increased the HTR and the pressure loss penalty.

The field synergy principle is a concept for convective heat transfer enhancement. This improvement is a synergy between the temperature gradient and velocity vector. An increase in the coordinate angle between the temperature gradient and velocity vector led an increase in the convective heat transfer. One way to improve coordination in the field is to create MLV in the fluid, as Guo ZY et al. [19] suggested. The velocity vector and temperature gradient $(V \cdot \nabla T)$ increased as θ increased.

In the θ of 40°, the pattern of streamlines is uniform, and they gradually changed as the angle increased. Also, the veloc-

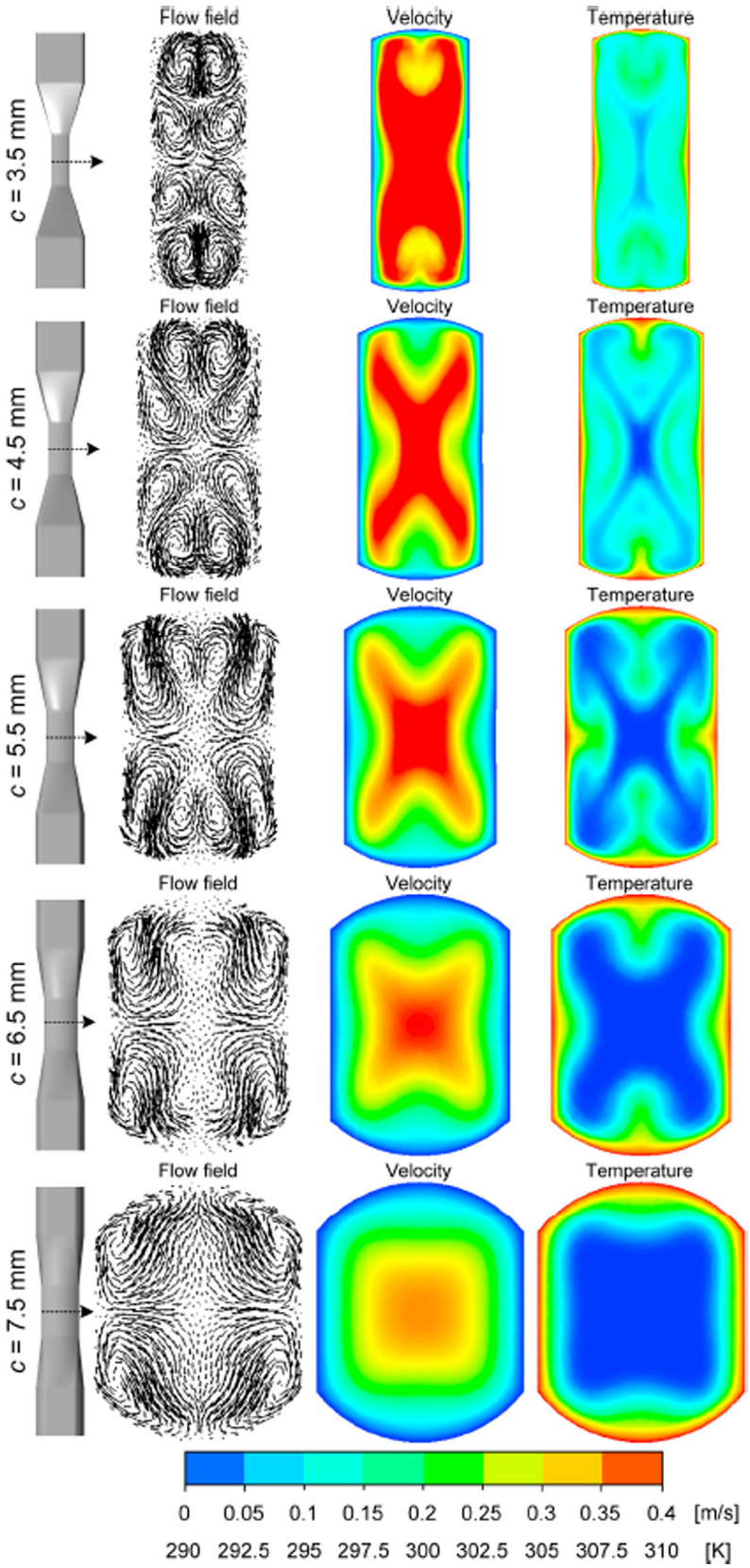

Fig. 12 Velocity pattern and temperature distribution for various AR [From Farsi et al. [25], with permission from Elsevier].

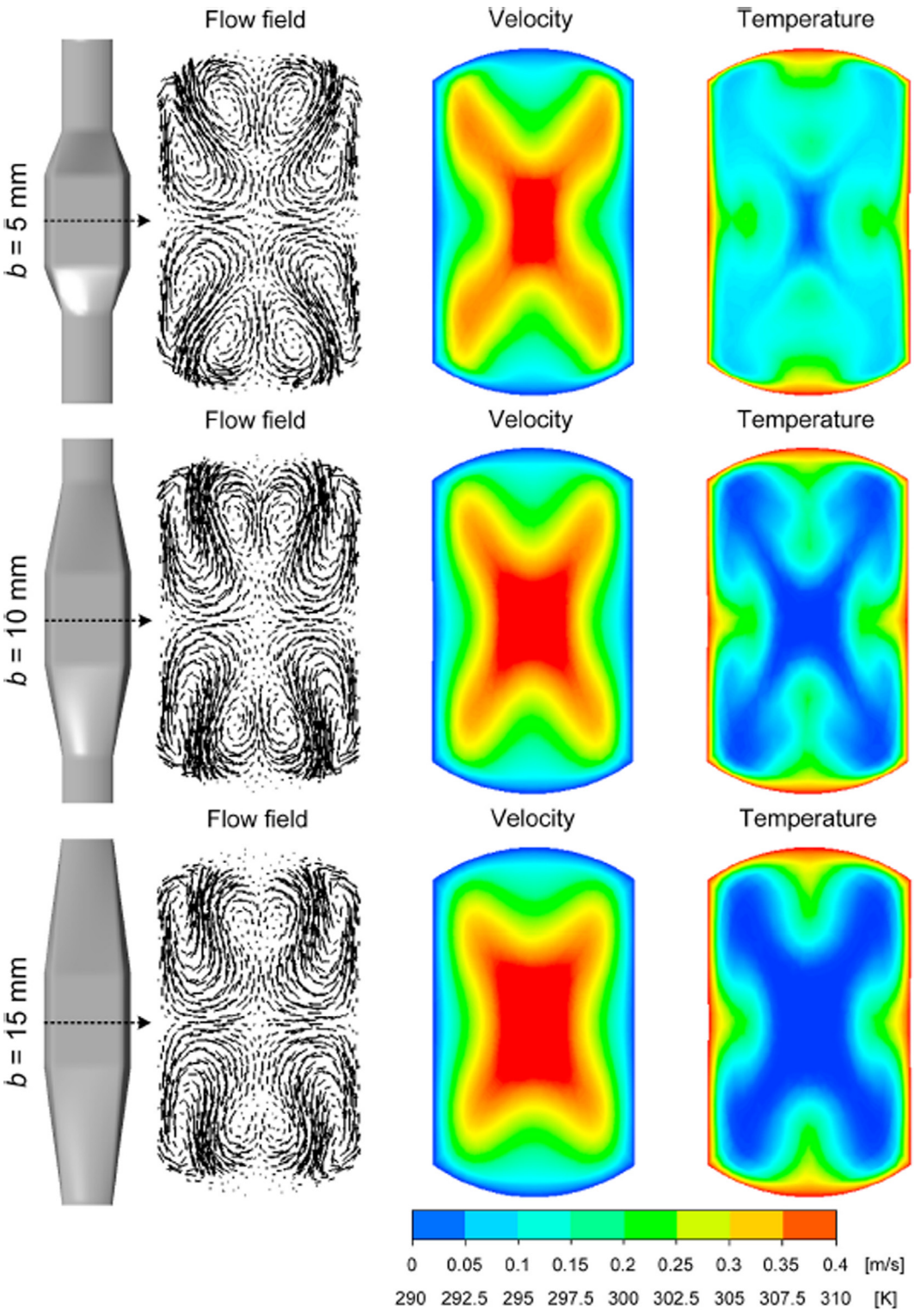

Fig. 13 Velocity pattern and temperature distribution for various TL [From Farsi et al. [25], with permission from Elsevier].

ity profile explaines the velocity distribution in various θ. In different axial directions, the distribution looked the same within the θ of 40°. On the other hand, when the angle increased due to the generation of secondary flow. Also, enlarging the θ resulted in the wall heat flux increased.

Also, Khaboshan and Nazif [37] indicated that an increase in the θ tended to increase the Nu and f. The Nu of the AEAT with θ of 40°, 60°, 80°, and 90° was 7.77%, 14.60%, 16.93%, and 24.42% higher, respectively, than those of the circular tube. The higher Nu came with a higher ΔP; however, the

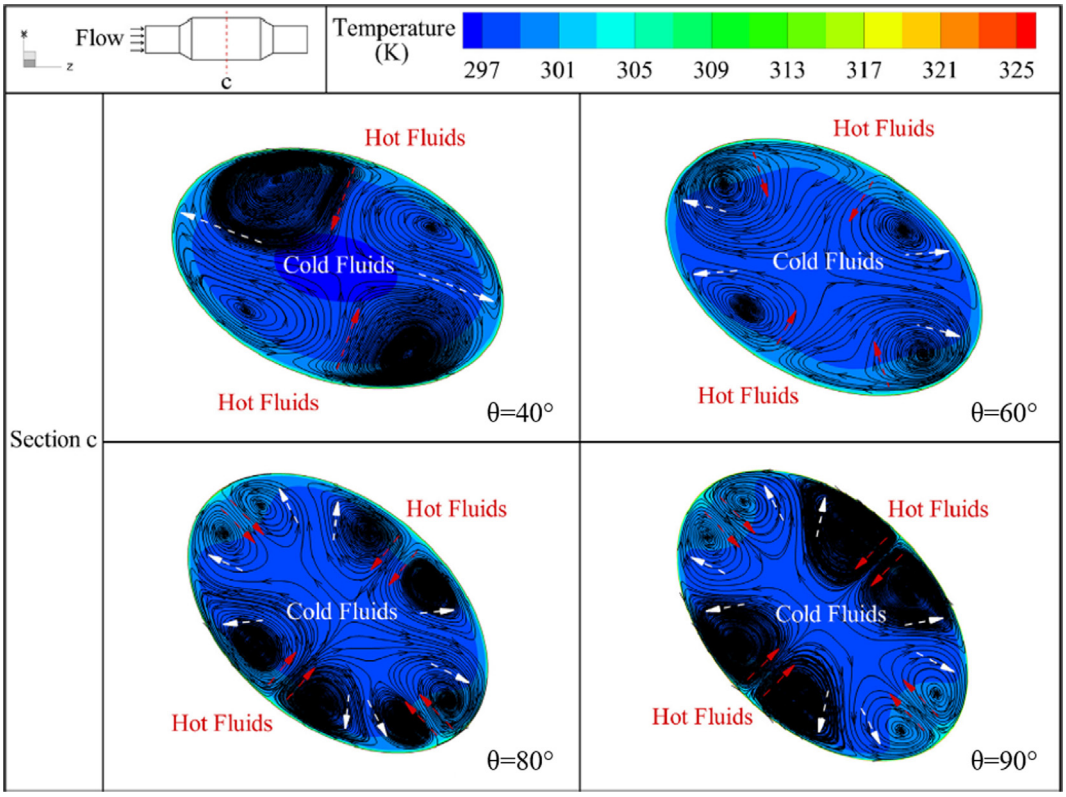

Fig. 14 Streamlines and temperature distributions on section c of the AEATs with the various alternating angles at Re = 40,000 [From Khaboshan and Nazif [35], with permission from Elsevier].

AEAT with the $\theta = 90°$ gave the highest ΔP. In the tube performance comparison, the AEAT was better than the circular one in the Re = 10,000. The best tube performance was obtained from the AEAT with the $\theta = 90°$, which performed about 1.09 times better than the circular one. However, the AEAT performance was not as good as the circular one for Re > 20000.

3.4. Miscellaneous parameters

The flow regime in the tube depends on the Re. Generally, the flow in the tube is a laminar flow for Re < 2,300 and turbulent flow for Re > 4000. However, flow characteristics in the ACT differ from the circular tube. The ACT can generate secondary flow by a deformed tube geometry. Evidently, Meng et al. [26] reported that the AEAT represented an early transition from a laminar flow regime to a low Re turbulent flow regime. Li et al. [20] used a simulation model to examine heat transfer and flow resistance of air flowing in an AEAT in the Re ranging from 200 to 20,000. The results showed that the fully developed laminar flow regime was mentioned as Re = 84.7. The transition from laminar flow to turbulent flow of the AEAT occurred at an early Re of approximately 1,000. Besides, Rukruang et al. [24] found that the entrance length of the turbulent flow was longer than that of the laminar flow as the susceptible turbulent flow deviated from the change of the cross-section of the tube. Also, the generation of vortices within the ACFT played a crucial role in improving the heat transfer characteristics, which accounts for the prominence of the HTC in the ACFT compared to the circular tube.

Two published papers were devoted to nanofluid flow in the ACT. The essential parameters, such as nanoparticle size and nanofluid concentration, were investigated. Khaboshan and Nazif [28] revealed that the HTC and ΔP increased by means of the addition of nanoparticles in a base fluid. Also, an increase to the volume fraction of the nanofluids and a reduction in the diameter of the nanoparticles tended to increase the $HTC_{avg,nf}/HTC_{avg,bf}$ and $\Delta P_{nf}/\Delta P_{bf}$ ratio, as well as the generation of the total entropy. At any inlet velocity, the friction irreversibility increases due to an increase in the nanoparticle volume fraction. Also, Sajadi and Talebi [23] denoted that the HTR increased as the concentration of the nanofluid increased. Compared with the base fluid, the HTR of Tube D (AR = 1.14) with 2% nanofluid concentration increased 20% and 16% for 400 < Re < 1800, respectively. Obviously, the ΔP of the AEAT was greater than that of the circular tube. An increase in the ΔP resulted from an increase in the concentration of the nanofluid. That is, the ΔP increased 6% and 14% for nanofluid concentrations of 1% and 2%, respectively.

3.5. Proposed correlations

As mentioned above, some researchers proposed correlations to predict Nu and f of ACT. For the AEAT, Meng et al. [26] developed Nu and f correlations within the Re range of 500 to 50,000 as below.

$$Nu_e = 0.0615\mathrm{Re}^{0.76}\mathrm{Pr}_f^{1/3}\left(\frac{\mathrm{Pr_f}}{\mathrm{Pr_w}}\right)^{0.11} \quad (1)$$

$$f_e = 1.54\mathrm{Re}^{-0.32} \quad (2)$$

Khaboshan and Nazif [35] proposed the correlations to predict the Nu and f in the Re ranging from 10,000 to 60,000, as follows.

$$\frac{Nu}{\mathrm{Pr}^{1/3}} = a'\mathrm{Re}^{b'} \quad (3)$$

$$f = a\mathrm{Re}^{b} \quad (4)$$

where the constant values are provided in Table 2.

For ACFT, Farsi et al. [25] also proposed correlations in terms of Nu and f. The correlations were valid for $500 < \mathrm{Re} < 1500$ with an average error within 5%. That is,

$$Nu = 0.02699\mathrm{Re}^{0.8602}\left(\frac{a}{b}\right)^{0.3186}\left(\frac{c}{d}\right)^{-1.4344} \quad (5)$$

$$f = 0.86921\mathrm{Re}^{-0.3790}\left(\frac{a}{b}\right)^{0.2574}\left(\frac{c}{d}\right)^{-2.7182} \quad (6)$$

where a is the pitch length, b is the transition section length, and c is the aspect ratio.

3.6. Benchmarking

In order to analogize the tube performance, a non-dimensional parameter, as the performance evaluation criteria (PEC), was employed. As discussed in the literature, compared to the circular tube, the ACT has better performance. That is because the ACT generated the eddy flow that made a well-mixed fluid inside the tube. Despite an increase in both the HTC and the flow resistance, the thermal performance of the ACT was superior to the pressure loss penalty. This was due to the distinctive coordination between the temperature and flow fields.

Meng et al. [23] compared the tube performance of twisted tape inserts and spirally corrugated tubes. The results were that the AEAT showed the best heat transfer enhancement with some additional ΔP for $\mathrm{Re} < 50000$. Sajadi et al. [33] indicated that the Nu and f of the ACFT are higher than those of the flattened tube by approximately 2–3 times and 0.6–1.5 times, respectively. Furthermore, Sajadi et al. [10] assessed the size of the heat exchanger by using an occupied space. The occupied space can be defined as the volume of the rectangular prism, which circumscribes the tube. Regardless of the length of the tube, this space can be determined as the rectangular area, which circumscribes the cross-section of the tube. However, the occupied space of the AFT appears to be the same as a flattened tube because it has the same cross-section. However, from the test results, the Nu and f of the AFT were higher than those of the flattened tube.

Table 2 Constant values for equations (3) and (4) [From Khaboshan and Nazif [35], with permission from Elsevier]

θ	40°	60°	80°	90°
a	0.8068	0.7898	0.5899	0.5625
b	−0.302	−0.282	−0.239	−0.225
a'	0.0406	0.0442	0.0414	0.0495
b'	0.7800	0.7778	0.7862	0.7749

4. Concentric tube

A few studies dealt with the flow and heat transfer characteristics of ACT in concentric tubes. In such studies, the fluid flow and heat transfer in an annular space with various tube configurations have been investigated. In addition, geometric parameters including the length of a heat exchanger, AR of ACT, and phase-shifting of a combined tube, were explored and discussed. In the following, some of these studies are summarized.

4.1. Flow behaviors at an annular space

Chen and Dung [38] used a numerical model to investigate flow behaviors in a concentric tube heat exchanger (see Fig. 15). The tube configurations were as (i) a circular tube was in an external part with an outer diameter of 33 mm, (ii) an AEAT was in an internal section with an outer diameter of 16.5 mm, and (iii) the tube lengths were 226, 306, and 386 mm. Chen and Dung described the presence of the velocity and temperature fields in a concentric tube under the constraint conditions: an internal velocity (V_i) of 0.0612 m/s, an external velocity (V_o) of 0.044 m/s, and a tube length (L) of 386 mm. V_i, V_o, Re_i, sand Re_o. Water was used as the working fluid for both external and internal sides. Vertical and horizontal cross-sections were selected at a mid-location of the tube length. The simulation results revealed an eddy flow in both vertical and horizontal cross-sections. A crucial flow characteristic to improve heat transfer was eddy flow or secondary flow.

In the horizontal and vertical cross-sections, four vortices were depicted in the external part of the annulus. The vortices were initiated from the TS region of an internal tube. At the TS, the vertical axis gradually transformed to the horizontal axis; Following an altered internal cross-section tube, the annular space gradually changed from expansion to contraction zones. As stated, the flow behaviors in the annular space illustrated an inverse phenomenon from the internal tube. Cross-sections with high pressure appeared in the horizontal direction, while cross-sections with low pressure showed up in the vertical direction. Finally, the vortices were formed at axial downstream of the TS. Velocity vectors and pressure contours through a transition section are depicted in Fig. 16.

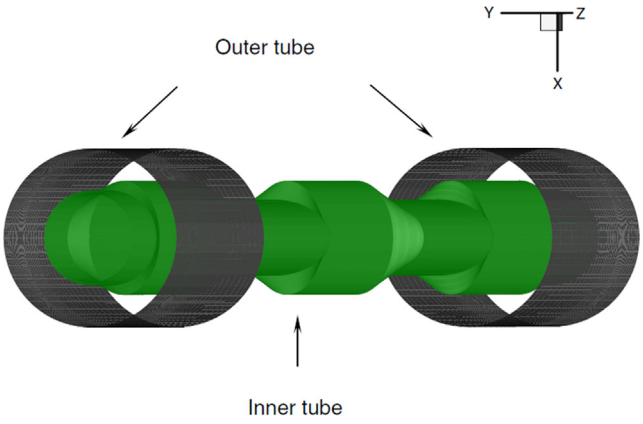

Fig. 15 Concentric tube configuration [From Chen and Dung [38], with permission from Elsevier].

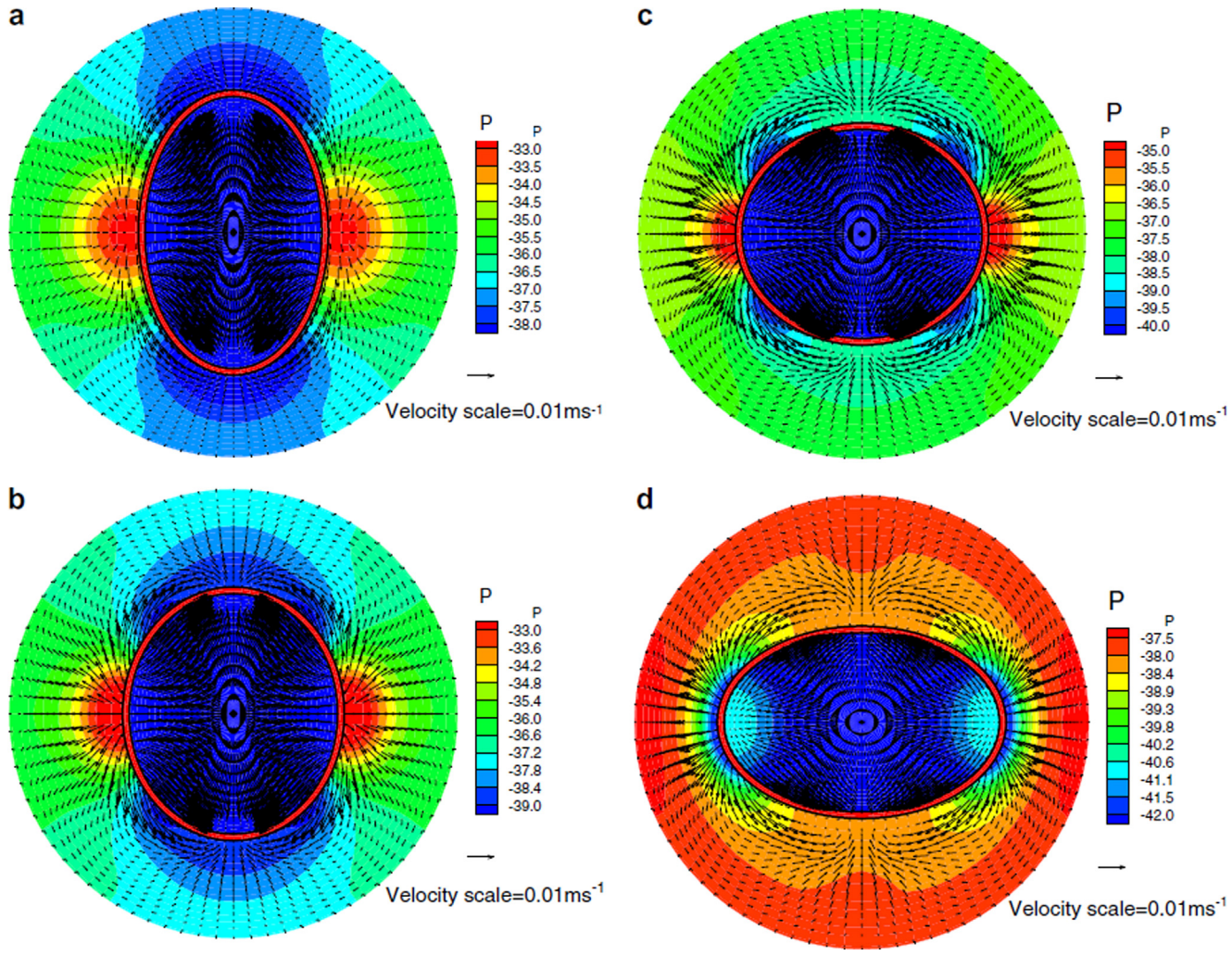

Fig. 16 Velocity vectors and pressure contours through a transition section withV_i = 0.0612 m/s, V_o = 0.044 m/s, and L = 386 mm: (a) beginning, (b) middle, (c) end, and (d) small distance downstream of the transition sections [From Chen and Dung [38], with permission from Elsevier].

Also, Vaezi et al. [39] examined the flow characteristics in the annular region of a concentric tube. This study applied the shortest concentric tube structure as provided by Chen and Dung [38]. They reported that the flow was accelerated in the horizontal cross-section and deaccelerated in the vertical cross-section. In the annular space, secondary flow formed from the horizontal axis to the vertical axis. Flow recirculation commonly appeared in the TS region, which increased the pressure loss and diminishing the HTR. Consequently, the pressure gradient was higher at the TS than in the other regions.

The mathematical investigation of fluid flow in an annular area was also conducted by Zambaux et al. [40]. They proposed a successive alternating wall deformation tube, where the tube arrangements at one wavelength were the section of a circular-vertical ellipse-circular-horizontal ellipse. From the tube structure, the successive alternating wall deformation tube can be imposed as the AEAT [41–42]. This study examined tube parameters within symmetry geometry. As a result, amplitude (A) and wavelength (λ) were used to represent AR and P. Tube configurations (Fig. 17) were (i) single external deformation (the AEAT as an external part and the circular tube as an internal part, as shown in Fig. 17a), (ii) single internal deformation (the circular tube as an external part and the AEAT as an internal part, as illustrated in Fig. 17b), and (iii) internal and external deformation (the AEAT as in both sides, as displayed in Fig. 17c). The AEAT consisted of 8 λ having a total length of 240 mm, and A of 1.25 mm. 30% mixture of glycol and water was used as working fluid at annular space.

Fig. 18 displays the velocity field in an annular region for a single AEAT and a combined tube. The AEAT as an internal tube (the first row of Fig. 18a), the eddy flow was induced by an internal tube: the flow drove from the vertical toward horizontal axis until the vortices formed in the horizontal area of the internal tube. Conversely, the AEAT as an external tube (the second row of Fig. 18a), the flow was pushed from the horizontal to the vertical axis; finally, the secondary flow was created in the vertical region of the external tube. It can be mentioned that the tangential velocity vector was an inverse direction to the AEAT's internal and external parts. The velocity intensity came to be opposite to $x/D_h = (7 + 1/4)\lambda$ and $(7 + 3/4)\lambda$. Deformation of the outer wall induced the

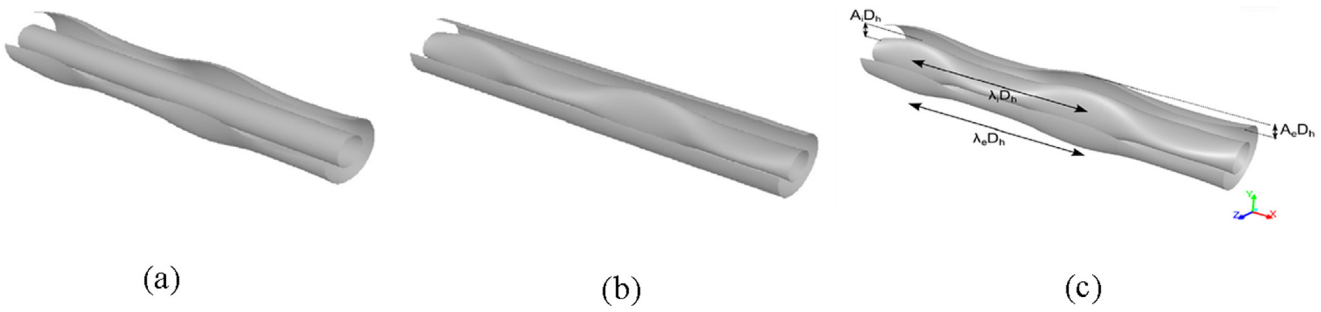

Fig. 17 The successive alternating wall deformation configurations: (a) single external deformation, (b) single internal deformation, and (c) internal and external deformation [From Zambaux et al. [40], with permission from Elsevier].

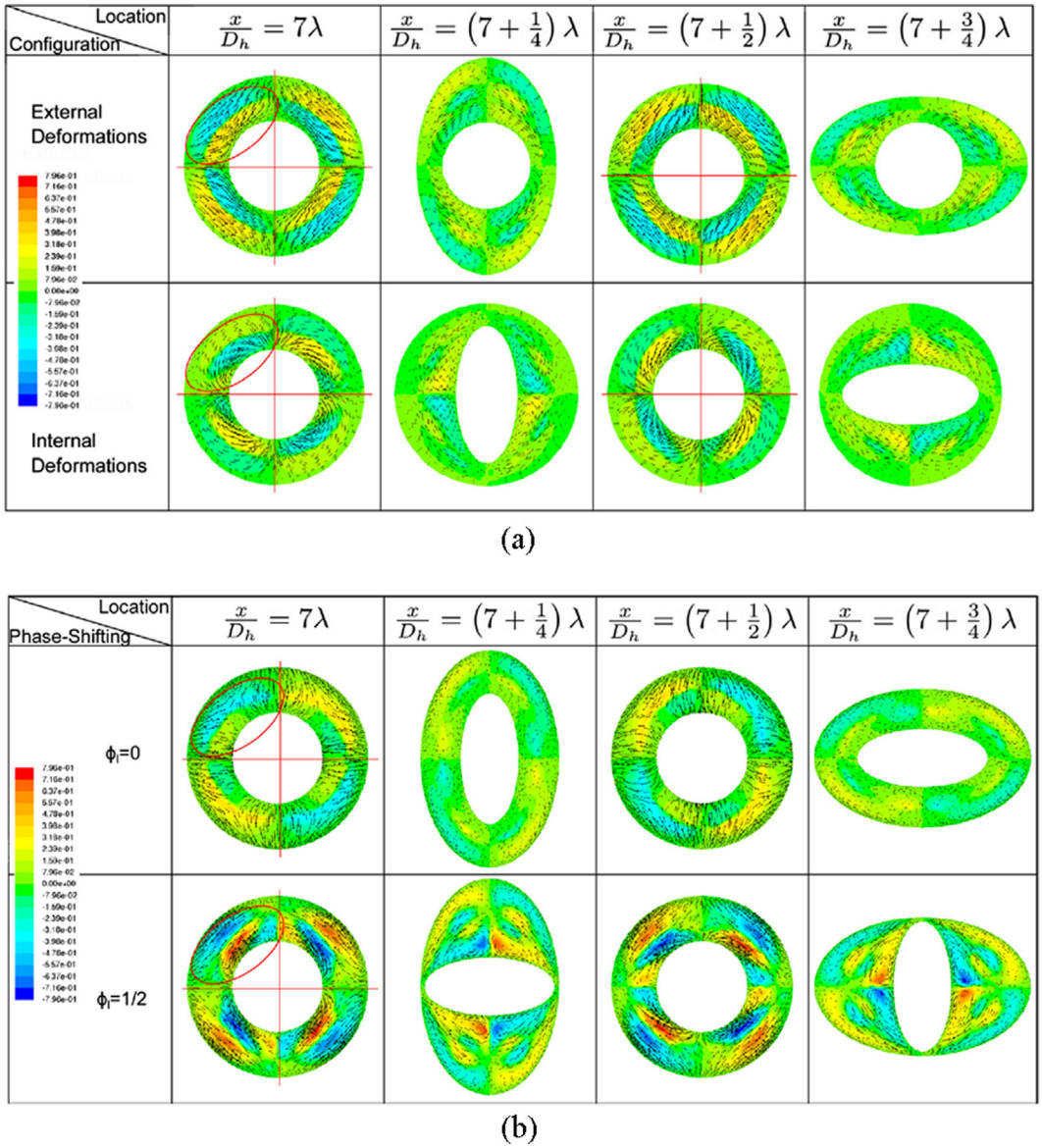

Fig. 18 Velocity vectors at an annular space: (a) a single wall deformation, (b) a combined wall deformation [From Zambaux et al. [40], with permission from Elsevier].

generation of vortices; contrarily, the tangential velocity vectors at the level of the internal deformations appeared in opposite directions. For the combined tube without phase-shifting ($\phi_I = 0$), The symmetry vertical and horizontal axes showed strong radial velocity, while the tangential velocity appeared weakly in those locations. Because the vortices were generated

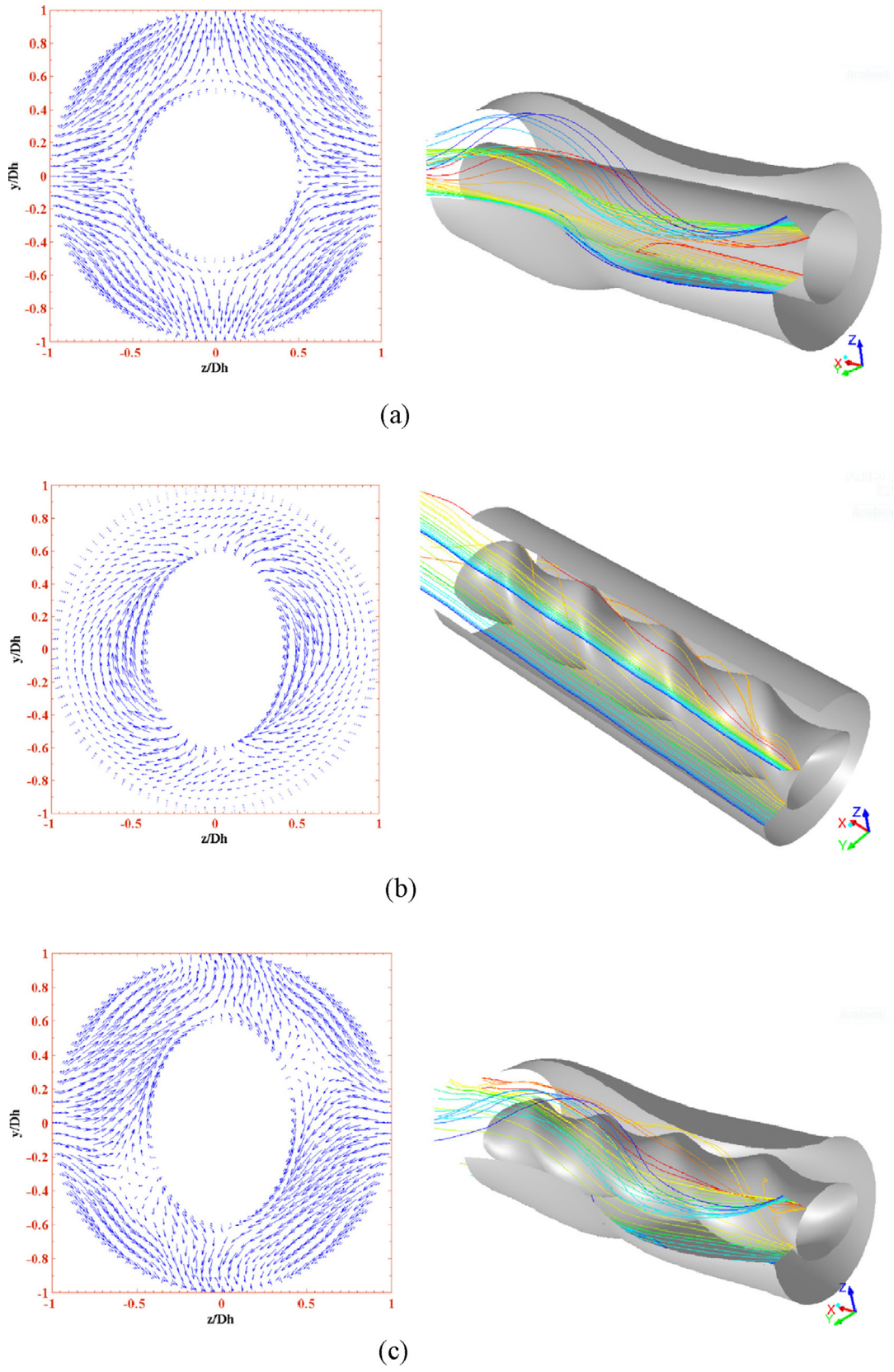

Fig. 19 Flow structure in an annular tube for Redial velocity vectors on a tube cross-section at $x = 11\lambda_e D_h$ and Trajectories of particles: (a) DET, (b) SC, and (c) DETSC [From Zambaux et al. [43], with permission from Elsevier].

from each AEAT having the same radial velocity direction, the longitudinal vortex structure was weakened. The maximum value of radial velocity was observed in the angular locations: 0°, 90°, 180°, and 270°, as presented in the first row of Fig. 18b.

This has been the continuous work of Zambaux et al. [43], related to three coaxial tube geometries, namely: (i) deformed external tube and smooth core or DET (Fig. 19a), (ii) smooth external tube and swirl core or SC (Fig. 19b), and (iii) deformed external tube and swirling core or DETSC (Fig. 19c).

Fig. 19 shows the flow structure in an annular space between three coaxial tubes. First (Fig. 19a), the DET appears as the strong velocity vector in a radial-axial direction. The trajectories show that the streamlines are distributed along the curved wall, and the vortex is expressed as a significant aspect in the longitudinal direction. Second (Fig. 19b), the SC produces the secondary flow in the tangential direction in which the flow was developed by the swirled inner tube. The eddy current travels along the region of the central wall; it results from the geometry of the swirled tube. It should be noted that it is impossible to see the flow movement in the radial-axial direction, which means a limit to the mixing efficiency of this geometry. Finally (Fig. 19c), the DETSC induced the velocity vector in the radial-axial direction. The flow characteristics become more complicated than those of the previous configurations. Moreover, it is observed that the radial movements from top to bottom were driven by the tangential movement. As a result, DETSC was an appropriate mixture that led to an increase in the heat and mass transfer.

4.2. Effect of ϕ_l on the thermal–hydraulic performance

As stated by Zambaux et al. [40], the flow characteristics in a combined AEAT (Fig. 17), the longitudinal vortices were weakened due to having the same radial velocity direction in each AEAT. Inverse flow behavior appeared in the phase-shifting configuration of $\phi_l = 1/2$. The ϕ_l was performed in the internal AEAT, which was defined in a spotted location in λ (1 λ can be split into 8 locations). The numerical results reported that the tangential velocity became a maximum value at the angular position of 45°, 135°, 225°, and 315°. The flow behaviors at an annular region occurred in the opposite direction due to having a different internal and external tube cross-section from the ϕ_l effect, as demonstrated in the second row of Fig. 18b.

The flow behaviors in an annular space were observed as radial velocity and tangential velocity, where each strong velocity occurred in a different angular position as an axis (0°, 90°, 180°, and 270°) and diagonal (45°, 135°, 225°, and 315°) locations. Regarding the $\phi_l = 0, 1/8, 7/8$, and 1, the main characteristics came from an influence of the radial velocity. On the other hand, the tangential velocity affected the flow at the $\phi_l = 1/4, 3/8, 1/2, 5/8$, and 3/4. Besides, the flow was in an inverse direction at the ϕ_l higher and lower values than 1/2. It caused from the flow direction changes to the opposite direction by a cross-section transformation.

In order to assess the heat transfer coefficient, the authors classified an interesting area into four regions, namely: (i) Region A ($0 \le \phi_l \le 1/8$), (ii) Region B ($1/8 \le \phi_l \le 1/2$), (iii) Region C($1/2 \le \phi_l \le 7/8$), and (iv) Region D ($7/8 \le \phi_l \le 1$). Region A presented a rapid increase in Nu, in which the radial velocity was strong and tangential velocity was more significant in this region. Region B showed that the Nu continuously increased at a reducing rate. Region C showed that the Nu dramatically decreased, which the tangential velocity became less important in this region. Moreover, Region D revealed that the Nu slightly decreased, in which the radial velocity became more important and tangential velocity was weakened. Comparing the performance of a combined AEAT with various ϕ_l, the optimum PEC was provided by a combined AEAT with $\phi_l = 1/8$. It was superior to a combined AEAT without ϕ_l ($\phi_l = 0$) and smooth annular by approximately 12% and 43%, respectively.

4.3. Effect of L and AR on the thermal–hydraulic performance

Chen and Dung [38] analyzed the thermal performance of a concentric tube with an AEAT inside by varing L. The thermal performances were represented by Nu, HTC, and enhancement ratio (ER). They reported that the Nu of a long tube was inferior to a short tube due to a longer middle section of the tube. Thus, the HTC both counter and parallel flow increased with decreasing L. In addition, the Nu gap between the AEAT and circular tube of a shorter tube was higher than a longer tube, resulting in a greater ER in a longer tube as the ER of 1.22 to 1.36 (which varied from L of 226 to 386 mm).

The variation of AR (AR of 1.3 to 2) was examined by Vaezi et al. [39]. Fig. 20 represents velocity and temperature

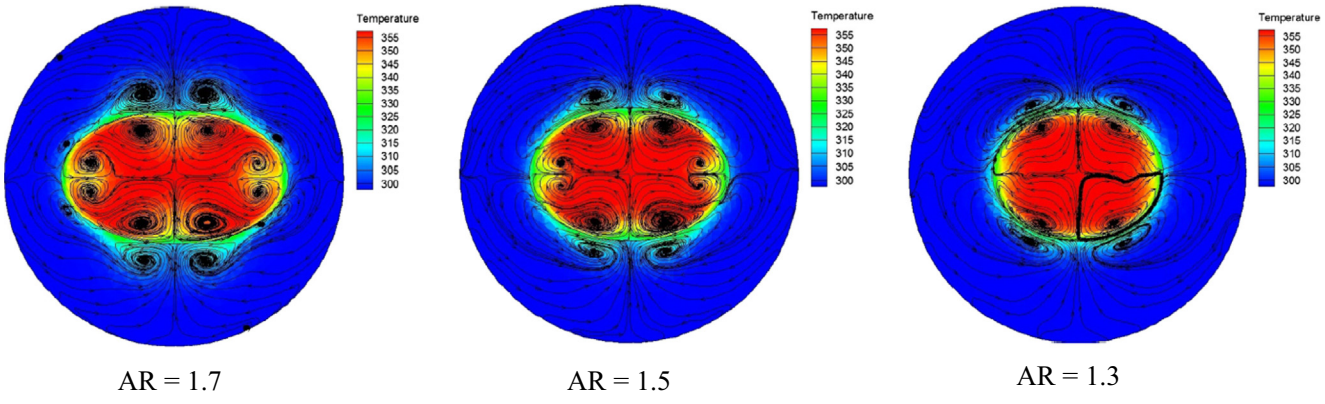

Fig. 20 velocity and temperature fields for various AR [From Vaezi et al. [39], with permission from Elsevier].

fields of various AR. An increase in AR created a recirculation zone in the TS. Also, an escalating in AR resulted in the size of separation bubble increased, which needed more pumping power to the system. However, an increase in AR resulted in the HTC augmentation; simultaneously, the friction loss also increased. A friction ratio ($f_{i,e}/f_{i,s}$ and $f_{o,e}/f_{o,s}$), above 1 indicates that an enhanced tube has more friction loss than a circular tube. Vaezi et al. [39] found that the friction ratio was lower than 1 at the lowest AR (AR = 1.3). In the internal tube, the friction ratio decreased with increasing the AR. On the contrary, the friction ratio increased with increasing the AR in the external tube.

4.4. *Effect of* Re_i *and* Re_o *on the thermal–hydraulic performance*

Chen and Dung [38] measured the Nu_{loc}, HTC_{oa}, and ER by varying the Re_i. The Nu at the entrance and end of the tube were higher than that at the middle of tube. Obviously, the TS region was a key to improve HTR in the AEAT. The HTC increased with increasing the Re_i as the ER of 1.068–1.35 (for counterflow) and 1.07–1.38 (for parallel flow). The tube performance was clearly improved with Re_i increased. Moreover, an increase in Re_o also led the HTC to augment; however, when the Re_o reached the maximum value, the HTC gradually decreased as the Re_o increased.

4.5. *ER map*

As mentioned, the AR, Re, and Reynolds number ratio (r) affected the thermal–hydraulic performance of the AEAT. Vaezi et al. [39] proposed the ER map for predicting AR_{min} and AR_{max} and finding the appropriate designed value of the AR. The ER map showed that the slenderized shape to be followed by decreasing r and increasing Re. An increase in Re tended to ΔP increased until it reached a greater value than the heat transfer enhancement, as exhibited in Fig. 21. Hence, an increase in Re and r led a region of ER greater than 1 to a narrow. The AR correlations were defined as:

$$AR_{\min} = a_0 + a_1 \mathrm{Re} + a_2/\mathrm{Re} + a_3 r \cdot \mathrm{Re} \tag{7}$$

$$AR_{\max} = a_0 + a_1 r \cdot \ln(\mathrm{Re}) + a_2 r + a_3 \ln(\mathrm{Re}) + a_4 r.\mathrm{Re} \tag{8}$$

where AR_{min} and AR_{max} gave the limit value of the AR that the ER greater than 1. Thus, the designed value should be selected from $AR_{min} < AR < AR_{max}$. The a_i variables are constant as shown in Table 3.

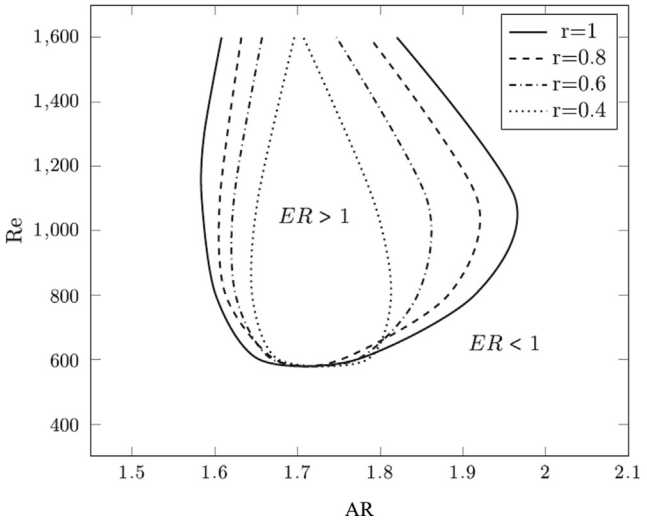

Fig. 21 ER map corresponding with the AR and Re [From Vaezi et al. [39], with permission from Elsevier].

5. Conclusion

Existing research solves the heat transfer problem through an improved tube called "alternating cross-section tube (ACT)." Most researchers have checked the thermal–hydraulic performance of the tube through numerical methods. Only one work was mentioned as an experimental approach. To study the heat transfer and flow characteristics, the tube configuration was evaluated. Although the ACTs produce a high-pressure drop, researchers have reported that the ACTs have a superior heat transfer performance than the round tubes. The important findings and research gaps in the literature review can be summarized as follows.

1. The ACTs can generate secondary flow and turbulence intensity through the tube curvature. The MLV developed along the length of the tube, which is an important improvement in the heat transfer performance of the tube. Also, the flow characteristics in the tube represent turbulent flow characteristics, leading to an early transition from laminar flow to turbulent flow at low Re.
2. Research parameters: AR, TL, and P are affected by heat transfer and flow characteristics. The HTC and ΔP increase with an increase in the AR, while the P and TL decrease. However, an increase in the AR can cause bubble separation in the transition region. This phenomenon tends to reduce the HTC and increase the ΔP. By designing appropriate geometric shapes to avoid separation in the transition region, flow resistance can be reduced.
3. The θ affected the flow behaviors inside the AEAT. Vortex generation was higher due to the increased θ from 40° to 90°. As a result, a larger θ increased the intensity of turbulence.
4. The nanoparticle size and nanofluid concentration were significant parameters that impacted the HTC and ΔP. The HTC ratio and ΔP ratio increased with decreasing nanoparticle size and increasing nanofluid concentration.

Table 3 Constant values for equation (7) and (8) [From Vaezi et al. [39], with permission from Elsevier]

AR	a_0	a_1	a_2	a_3	a_4
AR_{min}	1.27	2.34×10^{-4}	173	-9.25×10^{-5}	–
AR_{max}	2.84	1.62	−9.56	−0.164	-1.38×10^{-3}

5. In a concentric tube, the HTC_{oa} depended on the external and internal flow velocity. However, an increase in Re_i was more likely to improve HTC than an increase in Re_o. The flow behaviors in an annular space of an internal ACT were the opposite direction to an external ACT. In the laminar flow ($Re < 2{,}000$), the ER in parallel flow was slightly better than the counterflow, which was different from using a circular tube as an inner tube. The combined ACT has better thermal performance than the single ACT. The transformed cross-section created a swirling flow and induced a well-mixed fluid, resulting in an outstanding heat and mass transfer enhancement.
6. He literature review revealed that few studies explored the contribution of nanofluids to the performance improvement of ACT. Therefore, it is expected that by overcoming the barriers of nanofluid commercialization [44], more investigations would be performed on the effect of nanofluids on the performance of ACT.
7. The TS region commonly occurred a flow recirculation or bubble separation, which diminished the HTR of the ACT. Thus, to improve ACT performance, a designed ACT must avoid the presence of a recirculation zone. The smoothly transformed cross-section reduced bubble separation in the transition region due to reducing extreme expansion and contraction cross-section. Also, the ACT tube was combined with other passive enhancement techniques such as rough surface or extended surface.

Declaration of Competing Interest

The authors declare that they have no known competing financial interests or personal relationships that could have appeared to influence the work reported in this paper.

Acknowledgements

This work was supported by the National Research Council of Thailand (NRCT), Saijo Denki International Co., Ltd., and Research and Researchers for Industries (RRI) Ph.D. program [Grant no. PHD62I0029], National Science and Technology Development Agency (NSTDA) under the Research Chair Grant, and the Thailand Science Research and Innovation (TSRI) under the Fundamental Fund 2022.

References

[1] A. Bejan, A.D. Kraus, Heat Transfer Handbook, John Wiley & Sons, Inc., Hoboken, New Jersey, 2003.
[2] P. Błasiak, S. Pietrowicz, A numerical study on heat transfer enhancement via mechanical aids, Int. J. Heat Mass Transf. 140 (2019) 203–215.
[3] O. Ozkan, V. Bahadur, Heat transfer enhancement associated with electrostatic suppression of Leidenfrost droplets, Int. J. Heat Mass Transf. 149 (2020) 119207, https://doi.org/10.1016/j.ijheatmasstransfer.2019.119207.
[4] D. Zhang, E. Jiang, J. Zhou, C. Shen, Z. He, C. Xiao, Investigation on enhanced mechanism of heat transfer assisted by ultrasonic vibration, Int Commun Heat Mass Transf 115 (2020) 104523, https://doi.org/10.1016/j.icheatmasstransfer.2020.104523.
[5] A.S. Dalkılıç, O.A. Türk, H. Mercan, S. Nakkaew, S. Wongwises, An experimental investigation on heat transfer characteristics of graphite-SiO2/water hybrid nanofluid flow in horizontal tube with various quad-channel twisted tape inserts, Int Commun Heat Mass Transf 107 (2019) 1–13.
[6] H. Pourpasha, S. Zeinali Heris, O. Mahian, S. Wongwises, The effect of multi-wall carbon nanotubes/turbine meter oil nanofluid concentration on the thermophysical properties of lubricants, Powder Technol. 367 (2020) 133–142.
[7] S. Kakaç, A. Pramuanjaroenkij, Review of convective heat transfer enhancement with nanofluids, Int. J. Heat Mass Transf. 52 (13-14) (2009) 3187–3196.
[8] J. Kaew-On, K. Sakamatapan, S. Wongwises, Flow boiling pressure drop of R134a in the counter flow multiport minichannel heat exchangers, Exp. Therm Fluid Sci. 36 (2012) 107–117.
[9] N. Chimres, C.-C. Wang, S. Wongwises, Effect of elliptical winglet on the air-side performance of fin-and-tube heat exchanger, Int. J. Heat Mass Transf. 123 (2018) 583–599.
[10] A.R. Sajadi, F. Kowsary, M.A. Bijarchi, Y.D. Sorkhabi, S., Experimental and numerical study on heat transfer, flow resistance, and compactness of alternating flattened tubes, Appl. Therm. Eng. 108 (2016) 740–750.
[11] T. Chompookham, C. Thianpong, S. Kwankaomeng, P. Promvonge, Heat transfer augmentation in a wedge-ribbed channel using winglet vortex generators, Int Commun Heat Mass Transf 37 (2) (2010) 163–169.
[12] K. Wongcharee, S. Eiamsa-ard, Heat transfer enhancement by using CuO/water nanofluid in corrugated tube equipped with twisted tape, Int Commun Heat Mass Transf 39 (2) (2012) 251–257.
[13] S. Rainieri, F. Bozzoli, G. Pagliarini, Experimental investigation on the convective heat transfer in straight and coiled corrugated tubes for highly viscous fluids: Preliminary results, Int. J. Heat Mass Transf. 55 (1-3) (2012) 498–504.
[14] S.K. Saha, B.N. Swain, G.L. Dayanidhi, Friction and Thermal Characteristics of Laminar Flow of Viscous Oil Through a Circular Tube Having Axial Corrugations and Fitted With Helical Screw-Tape Inserts, J. Fluids Eng. 134 (2012).
[15] S. Ponnada, T. Subrahmanyam, S.V. Naidu, A comparative study on the thermal performance of water in a circular tube with twisted tapes, perforated twisted tapes and perforated twisted tapes with alternate axis, Int. J. Therm. Sci. 136 (2019) 530–538.
[16] N.H. Kim, E.J. Lee, H.W. Byun, Condensation heat transfer and pressure drop in flattened smooth tubes having different aspect ratios, Exp. Therm Fluid Sci. 46 (2013) 245–253.
[17] J. Kaew-On, N. Naphattharanun, R. Binmud, S. Wongwises, Condensation heat transfer characteristics of R134a flowing inside mini circular and flattened tubes, Int. J. Heat Mass Transf. 102 (2016) 86–97.
[18] J. Zhang, W. Li, S.A. Sherif, A numerical study of condensation heat transfer and pressure drop in horizontal round and flattened minichannels, Int. J. Therm. Sci. 106 (2016) 80–93.
[19] Z.Y. Guo, D.Y. Li, B.X. Wang, A novel concept for convective heat transfer enhancement, Int. J. Heat Mass Transf. 41 (14) (1998) 2221–2225.
[20] B. Li, B.o. Feng, Y.-L. He, W.-Q. Tao, Experimental study on friction factor and numerical simulation on flow and heat transfer in an alternating elliptical axis tube, Appl. Therm. Eng. 26 (17-18) (2006) 2336–2344.
[21] Z.Y. Guo, A brief introduction to a novel heat-transfer enhancement heat exchanger, Internal Report, Department of EMEMKLEHTEC, Tsinghua University, Beijing, China, 2003.
[22] W.R. Pauley, J.K. Eaton, The Effect of Embedded Longitudinal Vortex Arrays on Turbulent Boundary Layer Heat Transfer, J. Heat Transfer 116 (1994) 871–879.
[23] A.R. Sajadi, S. Talebi, Investigation of convective heat transfer, pressure drop and efficiency of ZnO/water nanofluid in alternating elliptical axis tubes, Environ. Eng. Sci. 8 (2020) 203–215.

[24] A. Rukruang, N. Chimres, J. Kaew-On, S. Wongwises, Experimental and numerical study on heat transfer and flow characteristics in an alternating cross-section flattened tube, Heat Transf Res 48 (3) (2019) 817–834.
[25] M. Farsi, M. Khoshvaght-Aliabadi, A. Alimoradi, A parametric study on heat transfer and pressure drop characteristics of circular tube with alternating flattened flow path, Int. J. Therm. Sci. 160 (2021) 106671, https://doi.org/10.1016/j.ijthermalsci.2020.106671.
[26] J.-A. Meng, X.-G. Liang, Z.-J. Chen, Z.-X. Li, Experimental study on convective heat transfer in alternating elliptical axis tubes, Exp. Therm Fluid Sci. 29 (4) (2005) 457–465.
[27] H. Najafi Khaboshan, H.R. Nazif, Numerical analysis on convective turbulent air in an alternating elliptical tube, Modares Mech Eng 16 (2017) 5–8.
[28] H. Najafi Khaboshan, H.R. Nazif, Heat transfer enhancement and entropy generation analysis of Al2O3-water nanofluid in an alternating oval cross-section tube using two-phase mixture model under turbulent flow, Heat Mass Transf. 54 (10) (2018) 3171–3183.
[29] W.-L. Chen, Z. Guo, C.-K. Chen, A numerical study on the flow over a novel tube for heat-transfer enhancement with a linear Eddy-viscosity model, Int. J. Heat Mass Transf. 47 (14-16) (2004) 3431–3439.
[30] W.L. Chen, L.-C. Fang, Numerical study on the flow over a staggered oval tube for heat-transfer enhancement, J Chinese Soc Mech Eng Trans Chinese Inst Eng Ser C/Chung-Kuo Chi Hsueh K Ch'eng Hsuebo Pao 25 (2004) 209–215.
[31] W.-L. Chen, A numerical study on the heat-transfer characteristics of an array of alternating horizontal or vertical oval cross-section pipes placed in a cross stream, Int. J. Refrig 30 (3) (2007) 454–463.
[32] W.-L. Chen, K.-L. Wong, C.-T. Huang, A parametric study on the laminar flow in an alternating horizontal or vertical oval cross-section pipe with computational fluid dynamics, Int. J. Heat Mass Transf. 49 (1-2) (2006) 287–296.
[33] A.R. Sajadi, S. Yamani Douzi Sorkhabi, D. Ashtiani, F. Kowsari, Experimental and numerical study on heat transfer and flow resistance of oil flow in alternating elliptical axis tubes. Int, J Heat Mass Transf 77 (2014) 124–130.
[34] H. Najafi Khaboshan, H.R. Nazif, Investigation of heat transfer and pressure drop of turbulent flow in tubes with successive alternating wall deformation under constant wall temperature boundary conditions, J Brazilian Soc Mech Sci Eng 40 (2018) 42.
[35] H. Najafi Khaboshan, H.R. Nazif, The effect of multi-longitudinal vortex generation on turbulent convective heat transfer within alternating elliptical axis tubes with various alternative angles, Case Stud Therm Eng 12 (2018) 237–247.
[36] H. Najafi Khaboshan, H.R. Nazif, Entropy generation analysis of convective turbulent flow in alternating elliptical axis tubes with different angles between pitches; a numerical investigation, Heat Mass Transf. 55 (10) (2019) 2857–2872.
[37] H. Najafi Khaboshan, H.R. Nazif, Numerical analysis of heat transfer enhancement and flow structure of alternating oval tubes by considering different alternate angles under turbulent flow, J Comput Appl Res Mech Eng 9 (2020) 211–223.
[38] W.-L. Chen, W.-C. Dung, Numerical study on heat transfer characteristics of double tube heat exchangers with alternating horizontal or vertical oval cross section pipes as inner tubes, Energy Convers Manag 49 (6) (2008) 1574–1583.
[39] S. Vaezi, S. Karbalaee M., P. Hanafizadeh, Effect of aspect ratio on heat transfer enhancement in alternating oval double pipe heat exchangers, Appl. Therm. Eng. 125 (2017) 1164–1172.
[40] J.-A. Zambaux, J.-L. Harion, S. Russeil, P. Bouvier, The effect of successive alternating wall deformation on the performance of an annular heat exchanger, Appl. Therm. Eng. 90 (2015) 286–295.
[41] Harion JL, Bertin JL, Bahadori B. Mixing and heat transfer increase in a tube with alternate successive deformations. W. H. E. W. P. Hahne, K. Spindl. (Eds.), 3rd Eur. Therm. Sci. Conf. 2000, Vol. 1, Ed. ETS, 2000, p. 331–6.
[42] Zambaux JA, Russeil S, Harion JL, Bouvier P. Numerical analysis of heat transfer increase in a tube with alternate successive gradual wall deformations. HEFAT2014 10th Int. Conf. Heat Transf. Fluid Mech. Thermodyn., July 14-16, 2014 Orlando, Florida.: 2014, p. 448–55.
[43] J.A. Zambaux, J.L. Harion, S. Russeil, P. Bouvier, Combining two orthogonal secondary flows to enhance the mixing in an annular duct, Chem. Eng. Res. Des. 94 (2015) 702–713.
[44] A. Alagumalai, C. Qin, V. K E K, E. Solomin, L. Yang, P. Zhang, T. Otanicar, A. Kasaeian, A.J. Chamkha, M.M. Rashidi, S. Wongwises, H.S. Ahn, Z. Lei, T. Saboori, O. Mahian, Conceptual analysis framework development to understand barriers of nanofluid commercialization, Nano Energy 92 (2022) 106736.